Published in final edited form as:
*Ind Eng Chem Res*. 2014 January 22; 53(3): 1130–1142. doi:10.1021/ie403353g.

# Iron-Based Redox Polymerization of Acrylic Acid for Direct Synthesis of Hydrogel/Membranes, and Metal Nanoparticles for Water Treatment

**Sebastián Hernández**, **Joseph K. Papp**, and **Dibakar Bhattacharyya***
Department of Chemical and Materials Engineering, University of Kentucky, Lexington, KY 40506-0046

## Abstract

Functionalized polymer materials with ion exchange groups and integration of nano-structured materials is an emerging area for catalytic and water pollution control applications. The polymerization of materials such as acrylic acid often requires persulfate initiator and a high temperature start. However, is generally known that metal ions accelerate such polymerizations starting from room temperature. If the metal is properly selected, it can be used in environmental applications adding two advantages simultaneously. This paper deals with this by polymerizing acrylic acid using iron as accelerant and its subsequent use for nanoparticle synthesis in hydrogel and PVDF membranes. Characterizations of hydrogel, membranes and nanoparticles were carried out with different techniques. Nanoparticles sizes of 30–60 nm were synthesized. Permeability and swelling measurements demonstrate an inverse relationship between hydrogel mesh size (6.30 to 8.34 nm) and membrane pores (222 to 110 nm). Quantitative reduction of trichloroethylene/ chloride generation by Fe/Pd nanoparticles in hydrogel/membrane platforms was also performed.

### Keywords

TCE; xerogel; iron nanoparticles; membrane functionalization; responsive behavior; catalysis

## 1 Introduction

Synthesis of polymers and polymer dispersions with different functional groups finds its application as templates for ion exchange, layer-by-layer deposition[1] or metal nanoparticle (NPs) synthesis.[2] In particular, cross-linked hydrophilic polymers which will convert from xerogel (dry) into a hydrogel (aqueous phase)[3,4] are extremely useful in these different functionalization processes.

A process for making these hydrogels is an acid-redox polymerization because of this process has high conversions (≥ 98%) and results in high molecular weight hydrogels. This polymerization is done in solution and/or using a bath to prevent overheating which gives a proper control of temperature[5] to arrest polymer gelation.[6–8] This acid-redox polymerization

*Corresponding Author: Prof. D. Bhattacharyya, University Alumni Professor, Department of Chemical & Materials Engineering, University of Kentucky, Lexington, KY 40506, db@engr.uky.edu, Phone No.: 859-257-2794.

includes strong oxidants like persulfates, perphosphates or peroxides and one or two reducing agents to initiate radicals. The reducing agents act as accelerants and can either be inorganic salts from metals like iron, copper, manganese, sodium, etc,[8,9] or organic salts. The organic salt such as ascorbic acid ($AH_2$)[6] has an added purpose of preventing the rapid oxidation of the metal ions by reducing them[10,11] and maintaining the production of free radicals.[12]

Due to their material versatility, hydrogels are used for NPs synthesis because hydrogels prevent trans-migration and aggregation. This contributes to increment the active surface area of the NPs along with their interfacial free energy and hence, their reactivity..[13,14] NPs are used because they have large surface area (and edge defects) compared with particles in regular metal powders. For making NPs inside a polymer, different types of process have been made like ion exchange[15–18], metal binding,[19] thermolysis,[20] crystallization[20,22] or metal inserts by sonochemical synthesis,[21].[21,22] Also during the polymerization, the NPs are encapsulated or used as a template to bind the polymer material.[3,23] The NPs immobilization is done because they cannot be recovered in solution phase due to their size; therefore a support is necessary to help in NPs immobilization and possible recycling.

Another advantage using hydrogels is the possibility of synthesizing them in different supports such as membranes, which has been discussed extensively.[24] The development of a functionalized membrane generates a good platform to synthesize metal nanoparticles (NPs) based on their inorganic salts. NPs in functionalized membranes have applications in different fields like electronics, mining, deionization, drug delivery detoxification of water and many more. [2] Specifically, iron NPs immobilization in membranes using different polymers have been reported by this research group and others [17,25]. [26] NPs with these specific properties are used in environmental applications such as transformation and capture of heavy metals[27] and elimination of chloro-organic toxic species.[28,29] So far, NPs immobilization in hydrogel and hydrogel/membrane systems has been achieved by using thermal (no redox) initiation in the process of polymerization.

Instead of thermal initiation, if a redox method of polymerization is performed, it can be used to maintain the added metal ions, which can be exploited to synthesize NPs inside the formed hydrogel. The main purpose of this study is to attempt to synthesize these NPs inside the hydrogel from the metal ions used in the hydrogel synthesis. With the synthesis of the NPs, this functionalized hydrogel could be applied in reductive/oxidative processes for water remediation. Based on this, specific objectives of the present work are: (1) to prepare a hydrogel of AA by acid redox polymerization; (2) to synthesize Fe NPs by using the remaining ferric and ferrous ions from the accelerant; (3) to characterize the immobilized NPs, the hydrogel produced and the membranes by different morphological, spectral and physico-chemical techniques; (4) to functionalize microfiltration (PVDF) membranes by the hydrogel synthesis within their pores and (5) to study the reactivity through the reduction of TCE by surface catalyzed reactions in aqueous solution.

# 2 Materials and Methods

## 2.1 Materials

Acrylic acid (AA, 99%), potassium tetrachloropalladate (II) ($K_2PdCl_4$, 98%), sodium borohydride ($NaBH_4$, 99.99%) (Sigma-Aldrich, St. Louis. MO, USA), ammonium persulfate ($(NH_4)_2S_2O_8$) (EM Science for Merck KGaA, Darmstadt, Germany); ferrous chloride tetrahydrate ($FeCl_2{\cdot}4H_2O$), ascorbic acid ($AH_2$), trichloroethylene (TCE = 99.9+ %), sodium hydroxide (NaOH) solution, sodium chloride (NaCl), sulfuric acid ($H_2SO_4$) solution and nitric acid (Fisher Scientific, Fair Lawn, NJ, USA); sodium borohydride ($NaBH_4$) (99.99%, Aldrich, St Louis, MO, USA); N, N'- methylenebisacrylamide (NMBA>99%) (Acros, New Jersey, NJ, USA); hydrophilized microfiltration polyvinylidene fluoride (PVDF) membranes of 650 nm pore size and 125 μm thickness (Millipore Corporation). In all cases 13.2 $cm^2$ membranes were used. All chemicals were of reagent grade and used as received.

## 2.2 Methods

**2.2.1 PAA synthesis and membrane functionalization—**All the quantities are molar percent based on the amount of monomer. Figure 1 serves as explanation of the polymerization, the membrane functionalization and NPs synthesis. In this process, 5 g of AA (monomer) was mixed maintaining constant stirring in 20 mL of DIUF water with NMBA (1.0%) as cross-linker and the initiator $(NH_4)_2S_2O_8$ (1.0%). $FeCl_2{\cdot}4H_2O$ (1.0%) and $AH_2$ (1.0%) were added in 20 mL of deoxygenated DIUF water. The polymerization is performed through a redox reaction of ferrous ion and $AH_2$ (accelerants/reductants) with persulfate ion (initiator/oxidant).[9,30] This method is started at room temperature (22–25 °C) and is exothermic. The pH is also a variable in the polymerization process, lower values (pH 2.0 to pH 6.0) are recommended using sulfuric acid or in this case, the monomer to control it. In this polymerization process the pH was 3.0.

The oxidant/reductants ratios of $S_2O_8^{2-}$: $Fe^{2+}$: $AH_2$ are 2:1:1 making the amount of iron selected suitable for polymerization[31]. The concentration of iron has to be the highest possible for direct NPs synthesis. However, compared to amounts used in other works is lower. The reaction with $AH_2$ is well known in redox polymerization by itself or using different metals, including iron.[9] The combination of this two reducing agents increase the rate of polymerization making the $AH_2$ and the $Fe^{3+}$ ion a redox pair, generating more initiating radicals. PVDF membranes were soaked in the monomer solution (Figure 1) while purging Nitrogen into it for about 30 min. Each membrane was put on a flat surface and sprayed with the initiator solution to begin the polymerization. For the hydrogel alone, the initiator solution was dripped on the monomer solution with constant stirring. Selected membranes and part of the hydrogel were washed to eliminate the unreacted material of the product and dried for 12 hr or until having constant mass for posterior ion exchange. The temperature of the reaction in the membranes was not controlled assuming the values of the solution reaction.

**2.2.2 Iron NPs production—**As illustrated in Figure 1, two procedures were performed. In the first one, the xerogel and the PVDF-PAA membranes were put in a solution of $NaBH_4$ (2.5 times molar excess) to reduce the iron present within the hydrogel that comes from the

redox polymerization. This is the direct NPs synthesis from the reducing agent. In the other procedure, the xerogel and the PVDF-PAA membranes were put in an alkaline solution of NaCl (1g/L of Na) to exchange the protons of the carboxylic groups from PAA by sodium ions. After 12 h, the materials are washed and put in a solution of $FeCl_2 \cdot 4H_2O$ (0.2 g/L of Fe). After washing with deoxygenated water, the reduction procedure is the same as the first. Pd is added to coat the iron, which increases the reactivity of the NPs giving a faster and complete dechlorination of TCE. To make bimetallic NPs, $K_2PdCl_4$ is used in concentrations between 1 to 5% following the reaction:[25]

$$Pd^{2+} + Fe^0 \rightarrow Fe^{2+} + Pd^0 \quad (1)$$

**2.2.3 TCE reductive dechlorination using Fe/Pd NPs—**TCE was selected as model pollutant. It is heavier than water, sinks bellow the ground water strata and is released very slowly making it very persistent in nature. However, TCE is a very volatile compound ($P^0$ = 0.08 bar), which makes it very difficult to study in continuous reaction processes. In previous works of this research group, convective flow experiments for dechlorination of TCE were performed, resulting in low correlations in mass balances due to the high volatility. For these reasons, convective flow dechlorinations were not performed. Fe/Pd NPs reactivity in hydrogel and membrane domain was determined by batch reaction with TCE. TCE solution is prepared by adding TCE liquid in deoxygenated water to make a solution of 30 mg/L of TCE. Batch experiments were conducted at 22–25 °C and pH = 6.0 in 43 mL and 120 mL vials for membrane and hydrogel, respectively. Functionalized membranes (13.2 $cm^2$ external area and 125 μm thickness non-functionalized) and a known weight of xerogel-NPs amount were soaked separately in the TCE solution and samples of liquid were collected at different time lapses with $N_2$ purge. Control experiments (no NPs) were also completed.

## 2.3 Material Characterization

**2.3.1 Determination of Fe content from catalyst and Fe/Pd loading in membranes—**For this step, the polymerization was made in solution putting the membranes on the bottom of the reactor in the monomer solution and then the $(NH_4)_2S_2O_8$ solution was dripped into it (0.5 mL/min). To determine the ratio of $Fe^{2+}/Fe^{3+}$ within the hydrogel and the membranes after the polymerization process, samples were put in a solution of HCl 0.2 M to prevent oxidation of ferrous ions for 12 hr in 20 mL EPA glass vials and then spiked for analysis with Iron Standard solution. The concentration of ferrous ions was measured by the Ferrozine method[32,33] in an UV-Visible spectrophotometer (Varian Cary 300 Bio) setting the detection at 562.0 nm with analytical error of 1%.

Total iron was determined by digesting the solutions from the monomer solution and membranes in nitric acid. 20 mL EPA glass vials were used and the iron concentration was measured by atomic absorption spectrometer (AA) (Varian SpectrAA 220 Fast Sequential) with a Fe lamp detector at 386.0 nm and an analytical error of 2%. The amount of iron in the hydrogel was determined by material balance. The same procedure was performed for the determination of Pd (at 244.8 nm) content in the functionalized membranes and the hydrogel.

**2.3.2 Polymer analysis by FTIR and ATR-FTIR—**The xerogel was analyzed using a Fourier transform infrared spectroscopy (FTIR) (Thermo-Nicolet Nexus 470 FT-IR ESP). The hydrogel/membrane system was analyzed with an Attenuated total reflectance FTIR (ATR-FTIR) (Varian 7000e) to validate qualitatively the presence of chemical functional groups. The spectrum was set between 500 and 4000 $cm^{-1}$.

**2.3.3 Morphology of the hydrogel, membranes and NPs—**The morphology of the hydrogel (as xerogel), the membranes and the NPs inside were observed and analyzed using a scanning electron microscope (SEM) Hitachi S4300, operated at accelerating voltage from 3 to 20 kV for the hydrogel and the membranes. Before any SEM analysis, the samples were dried in a freeze-vacuum-drier LABCONCO FreeZone 2.5 Plus.

**2.3.4 Elemental composition of hydrogel and membranes—**To measure the elemental composition, samples were analyzed with an energy dispersive X-ray spectrometer (EDS) in a SEM Hitachi S-3200N. In addition, X-ray photoelectron spectroscopy scans were performed with (Thermo Scientific K-Alpha XPS System) to measure the elemental composition on the surface of the hydrogel and hydrogel/membrane systems. For the latter system, an additional etching was performed to elucidate the variation in composition through the membrane profile.

**2.3.5 Determination of swelling degree—**The produced hydrogel is washed with DIUF water until constant pH and then vacuum dried until constant weight. Then, the xerogel is immersed in different pH buffer solutions ($1.9 \leq pH \leq 9.3$) at constant temperature (22 °C) absorbing until the weight remains constant. Each sample of hydrogel was tested to calculate the changes in the diffusion characteristics due pH changes and thus, correlate them to the responsive behavior in the functionalized membranes. The amount of water absorbed and retained by the hydrogel at constant temperature and pH can be expressed by:[34]

$$W = \frac{water\ content\ in\ hydrogel}{total\ weight\ of\ hydrogel} = \frac{m - m_0}{m} \quad (2)$$

where $m_0$ and $m$ are the weights of the xerogel and the hydrogel, respectively. Its behavior is asymptotic when $W$ tends to the unit reaching the highest water uptake possible in equilibrium, $W_{eq}$.

**2.3.6 TCE reduction analysis—**TCE content of each sample was extracted with an equal volume of pentane with 1, 2-dibromoethane (EDB) (0.116 mM) as internal standard for 2 hr and analyzed by Gas Chromatography – Mass Spectrometry (GC-MS) (Hewlett-Packard Series II 5890 GC-MS) with helium as carrier gas. A calibration curve was created with different solution values varying from 10 mg/L to 40 mg/L with a linear $R^2 = 0.989$ and an error < 3%.

# 3 Results and Discussion

## 3.1 Polymerization

**3.1.1 Reaction Mechanisms—**The polymerization of AA by redox couples of $Fe^{2+}$ or $AH_2$ with $S_2O_8^-$ are discussed in different works with polymeric products with high molecular weight due to cross-linking. Reported data showed values of molecular weight of $M_n >> 5000$, only for acrylic acid polymerizations.[35] However, the utilization of this redox system was reported so far in one experimental work[36] and is mentioned in polymerization reviews referenced. The production of free radicals in this system is governed by 2 equations (adapted from Sarac[9]):

$$Fe^{2+} + S_2O_8^- \rightarrow Fe^{3+} + SO_4^{-\bullet} + SO_4^{2-} \quad (3)$$

$$AH_2 + S_2O_8^- \rightarrow A^{\bullet}H + 2H^+ + SO_4^{2-} \quad (4)$$

Ferrous ions start to oxidize creating sulfate radicals from persulfate and at the same time this compound starts to form ascorbate radicals (Equations 3 and 4). The PAA starts to aggregate very fast forming a more dense material, which starts to absorb all the solution around it. The pH tends to be stable because of the ionization of the AA and $AH_2$. The reaction is heterogeneous and depends on the initiators and the monomer concentration with ½ and 3/2 power, respectively.[8,35]

Some side reactions take place during the polymerization. The most important is the reduction of $Fe^{3+}$ by $AH_2$ (Equation 5). This reduction induces the generation of more sulfate radicals by production of $Fe^{2+}$ ions, increasing the polymerization efficiency (high conversion) and leaving dehydroascorbic acid (A) as byproduct in a low pH environment. However, sulfate radical can be diminished by the $Fe^{2+}$ formed (Equation 6), it also can be created by chain transfer from the growing chain $M_n^{\bullet}$ to persulfate (Equation 7) or disappear by coupling (Equation 8). Those two reactions give possibly short length chains of polymer.

$$2Fe^{3+} + AH_2 \rightarrow 2Fe^{2+} + 2H^+ + A \quad (5)$$

$$SO_4^{-\bullet} + Fe^{2+} \rightarrow Fe^{3+} + SO_4^{2-} \quad (6)$$

$$M_n^{\bullet} + S_2O_8^{2-} \rightarrow Polymer + SO_4^{-\bullet} \quad (7)$$

$$M_n^{\bullet} + SO_4^{-\bullet} \rightarrow Polymer \quad (8)$$

**3.1.2 Temperature, pH and iron content—**The increment in the temperature of the polymerization over time tends to a plateau as a result of the exothermic redox reaction. Temperatures around 50 °C for a reaction surrounded by water in an external vessel at 15 °C, and a faster reaction at ≈ 60 °C without water surroundings are reached. These

temperatures are recognized by different studies in which the conversion reaches around 85% of the initial monomer concentration and were heated at the same or higher temperature.[35,37,38] By adding the initiators dropwise, it was suitable to control the temperature increment for hydrogel synthesis alone. The higher temperature reached was assumed for the membrane functionalization, since its control was not technically feasible.

The ratio of iron used for polymerization was 1:100 molar based on the monomer which is lower than the used in the ion exchange procedure, which is 1:2 to make NPs. The iron form is mostly ferric instead of ferrous due to the oxidation from the initiation, confirmed by the data from the Ferrozine method (Table 1). Its characteristic brown color (See Figure 1) is due to the reaction of the hexaaquairon(III) ion formed with water. This reaction contributes to the decreasing in the pH by pulling off hydrogen atoms into water. In addition to this, the polymerization goes to a minimum (pH = 2.0) as a result of the ionization of $AH_2$ and AA. The reduction of iron ions takes place immediately without wash, implying that ferrous and ferric ions stayed in solution before reduction. This reduction of iron to form NPs needs a $NaBH_4/Fe^{3+}$ ratio of 3:1 or 3:4 compared to 2:1 $NaBH_4/Fe^{2+}$ from the ion exchange (see Equations 9 to 11).[39–41] The pH of the reduction was around 9.0 and the hydrogel synthesized had anionic behavior, which could show presence of ferrous hydroxide (precipitated).

$$Fe^{2+}+2BH_4^-+6H_2O \rightarrow Fe^0+2B(OH)_3+7H_2 \quad (9)$$

$$BH_4^-+2H_2O \rightarrow BO_2^-+4H_2 \quad (10)$$

$$Fe^{3+}+3BH_4^-+9H_2O \rightarrow Fe^0+3H_2BO_3^-+12H^++6H_2 \quad (11)$$

Table 1 shows the amounts of iron in each procedure. From the polymerization of the hydrogel alone, the iron obtained (9.2 mg Fe/ g PAA) was higher to the calculated (7.75 mg/ g PAA). After ion exchange, the amount of iron after ion exchange in the hydrogel (450 mg Fe/ g PAA) was also higher (387.5 mg/ g PAA) due to two different factors: first, the higher swelling capacity of the hydrogel which increases the iron adsorption and second, the possible residual iron from polymerization. On the other hand, the amount of iron after polymerization inside the membranes was lower. One of the reasons of this result is that the mass gain of the membranes by the polymerization was between 8.5 and 13.4% but this represents only about 1.0% of the total reactive solution.

The percentage of PAA within the PVDF membrane showed less potential for iron loading compared to the hydrogel only. This is because most of the polymerization occurred on the membrane surface due to faster rates of redox reaction; this decreases the active area of the membranes and promotes losses of iron once the membrane is put in solution. The ion exchange process of $Na^+$ by $Fe^{2+}$ ions is at lower pH than the exchange of $H^+$ by $Na^+$ which implies less swelling, influencing additional iron loading. The amount of iron inside each PVDF-PAA membrane ranged between 1.4 and 4.2 mg / 13.2 $cm^2$ membrane after ion exchange. This value is higher than the amount obtained from direct hydrogel synthesis but

less than the achieved by other studies..[25,42,43] However, the iron loading obtained with respect to carboxylic groups is near the calculated of 1:2. This suggests the impossibility of higher iron loading due to space limitations within the pore. In addition to that, the chelating behavior of the ascorbic acid in the solution and the repulsion of the counter ions with the carboxylic groups could also influence the lower concentration of iron in the membrane.

### 3.2 Cross-linked PAA Hydrogel, PVDF-PAA membranes and NPs characterization

Cross-linked PAA synthesis was conducted at known temperatures which give a very stable material under basic or acid conditions. These properties combined with the excellent chemical resistance of PVDF to broader types of agents (acid, weak alkaline and oxidizing) generate a very versatile material. Based on the FTIR and ATR-FTIR spectrums, the polymerization and functionalization can be confirmed. From Figure 2, a comparison between commercial PAA powder and the hydrogel indicates the synthesis of the hydrogel, showing a strong wide band in the region of 3300–2500 $cm^{-1}$ and demonstrating presence of O-H groups. For PAA powder, at 1700 $cm^{-1}$ the C=O group is defined (Figure 2a). Due to the washes after polymerization, the hydrogel can be ionized[44,45] and show two defined peaks between 1750 and 1600 $cm^{-1}$ related to C=O from the carboxylic acid (-COOH) and carboxylate ($-COO^{-}$) groups, respectively (Figure 2b). The spectrums of the functionalized membranes compared to the bare PVDF (C-F/C-$F_2$ groups between 1100 and 1500 $cm^{-1}$) in Figure 3 show the addition of the C=O at 1740 $cm^{-1}$, and broad peaks between 3000 and 2500 $cm^{-1}$ demonstrating the presence of O-H from the hydrogel synthesized (Figure 3b). The presence of brown color due to the presence of hexaaquairon(III) diminishes the transmittance by an unclear signal, reflected in the noise of the spectrums showed in the sole hydrogel and the functionalized membranes.

The morphology of the bare xerogel surface looks wrinkled, porous, and open in the Figure 4a-b. The lower voltage for the observations of the gel are because this material is not very stable at high voltages and can burn especially at low cross-linking degree. PAA as polyelectrolyte has a very good ion exchange capability at neutral to lower basic pH and its pKa is similar to AA (pKa = 4.7).[46] Based on the quantities of iron and polymer used in the ion exchange, molar $COOH/Fe^{2+}$ ratios were between 2.04 and 5.9 to 1. The first value is near the calculated ratio of 2 and demonstrates higher uptake of iron from ion exchange. The second value shows lower iron loading due possibly to transport phenomena and poor ion exchange with the sodium used. The amount of iron taken by ion exchange is higher than the one obtained only by polymerization itself, going from 9.2 to 457.5 mg Fe/g PAA (Table 1). However, the calculated amount of iron could be near 830 mg/g PAA based on the sodium exchanged which indicates higher capacity due to swelling rather than to ion exchange processes.

From a comparative survey done with the XPS to the xerogel from thermal and redox polymerization (Figure 5 a-b, respectively) it is revealed the presence of oxygen and carbon in the former and a low amount of sulfur in the latter. Sulfur (from sulfate) as initiator in both reactions has higher concentration in the redox initiation, which is confirmed here. In the xerogel from redox initiation, the ratio between oxygen and carbon is near to the

stoichiometric value (2:3) but is lower in the thermal sample due possibly to low ionization from the XPS equipment.

Posterior to reduction, NPs were formed on the surface and the pores of the hydrogel. In the pores NPs are more widely distributed (Figure 6a) and most of the aggregates are located in the surface (Figure 6b). These figures demonstrate that the immobilization prevents NPs aggregation and also demonstrate that the synthesis of NPs from the accelerant used in the polymerization is possible. The SEM images show that the NPs size goes from 30 to 60 nm.

Bare PVDF membrane (Figure 7a) shows a porous structure and the thickness is around 120 μm (125 μm from manufacturers data). After polymerization, the hydrogel spreads in the whole porous media of the membrane (Figure 7b), covering several areas at the interior of the membrane structure. On the surface, PVDF membrane (Figure 7c) appears more open than the PVDF-PAA (Figure 7d) that has a cover of polymer on the surface. PVDF has a nominal diameter of 650 nm according to manufacturer's data. The PVDF-PAA pore size was calculated from SEM images measuring the pore sizes in a defined area and generating an average value of 690 ± 58 nm. In addition, an analysis of the pores at higher magnification after polymerization (Figure 7e) and after reduction (Figure 7f) showed pore sizes near 600 nm. These are lower than the bare PVDF membrane due to some polymer formed on the surface.

XPS comparative spectrums of the membranes show that the fluorine/carbon ratio is near to the PVDF value (1:1) with a decrease due to the presence of carboxylic groups (Figure 5 c-d). In the Figure 5 d, is also shown a presence of iron and a small amount of nitrogen on the surface of the membrane that is not perceived in the xerogel alone. The explanation for this phenomenon is that iron diffuses from the interior of the membrane to encounter the sulfate radical and the reaction initiates on the surface. Although this happens on the hydrogel system too, is more notorious in the membrane due to the mobility restriction within the pores. This also could explain the low amount of iron inside the membranes.

Prior to the surface analysis, an etching procedure with an argon ion gun was performed. This procedure only analyzes the surface of the material and penetrates a few nm. However, it can show the trend of the elements composition through the material. The results of the XPS etching are shown in the Figure 8a. These show that the oxygen is more present on the surface of the membrane and decreases to a stable value of 13%. The amount of fluorine tends to be stable around 11%. Due to the presence of oxygen, the ratio of fluorine/carbon decreased from the theoretical 1:1 for PVDF to near 1:5 for the PVDF-PAA (Figure 8b). The etching shows that, although the polymerization takes place in the surface level, it spreads into the membrane's interior. On the other hand, the amount of iron is stable lengthwise too with a value of 0.25%, which is lower than the one on the surface of 2.47% (Figure 5d). This also confirms the diffusive behavior of iron to initiate polymerization.

After ion exchange and posterior reduction to form NPs, the structure of the membrane surface was less porous (for PVDF-PAA-Fe is 317 ± 55 nm) due to swelling stresses produced by the pH change in the $NaBH_4$ reduction. The membrane surface (Figure 9a) and cross-section (Figure 9b) show that the size of the particles are also between 30 and 60 nm.

The membrane support along with the gel verifies a decreasing in particle agglomeration and the presence of iron is confirmed by EDS analysis from Figure 10. The binding energy of iron is in the range of 7 keV, which confirm the presence of iron (Figure 10a). As it is shown in Figure 10b, some sodium is still in the membrane from the sodium borohydride and ion exchange processes (33% of Fe compared with 8% of Na). The mapping of the elements also accentuates the iron, carbon and fluorine on the surface of the membrane (Figure 10c) while oxygen is under-lapped. Assuming a particle size of 60 nm with spherical size and uniform distribution, the specific surface area of the NPs is around 12.7 $m^2/g$.

### 3.3 Hydrogel structural and physicochemical characterization

The lattice size of a hydrogel is altered drastically with small pH changes. When the pH of cross-linked PAA is raised above its pKa, a charged repulsion of the carboxylic groups is created expanding the size of the hydrogel and increasing the swelling degree. When the pH is lowered, the charged repulsion phenomenon is the opposite and the swelling is lower. Since the membranes are modified with this material, swelling studies were done to demonstrate the relationship of pH response in the hydrogel to the change in the pore of functionalized membranes.

With the experimental data of water uptake by the hydrogel, the isothermal swelling degree calculated by the amount of water retained $W$ is plotted as a function of time in Figure 11. All the samples showed similar behavior, increasing the water content drastically at the beginning, reaching a plateau after certain time. For the hydrogel fabricated by redox polymerization (Figure 11a), the plateau was reached in 15 min or less. Except for pH 1.9, which plateau, was reached after approximately 50 min, due to the tight structure of no-repulsion between carboxylic groups. Then, the increment in water content was more slowly until equilibrium was reached ($W_{eq}$), showing higher amounts of buffer solution absorbed at higher pH values for both hydrogels.

In the hydrogel made by thermal polymerization, the plateau was reached more slowly at almost 500 to 1000 min. The very high responsive behavior from the former hydrogel is a direct consequence of the electrolytes present within, due to the species involved in the synthesis. The absorption capacity of the hydrogels at equilibrium showed that the weight gain percentage with respect to the xerogel when swelling occurs goes from 213% at pH 1.9 to 776% at pH 9.3, in the one made by redox and from 194% to 1676% in the same range of pH. The first results are low compared to literature[46] and could be a consequence of the redox polymerization process and the presence of highly cross-linked sites in some parts of the material. In addition to that, these results agreed with different works that show lower capacities in the presence of more concentrated solutions.[47,48]

To establish the swelling behavior, first-order and second-order swelling kinetics models were considered (Equations 12 and 14). The first-order kinetics is similar to the obtained by Fick's law of diffusion in one-dimensional swelling of films for long times, which assumes diffusion coefficient and thickness of the film constant during the swelling process. Based on that, is predictable, that the first-order will not fit the experimental data due to the changes in the swelling and volume of the material with time.[49] After integration of each model (Equations 13 and 15), only the second-order model fits the experimental data.

Shown in Figure 12 with $R^2$ between 0.999 and 1.000, the rate of swelling of the cross-linked PAA hydrogel is proportional to the quadratic of swelling capacity offered, making the swelling process faster at higher pH values.

$$\frac{dW}{dt} = K(W_{eq} - W) \quad (12)$$

$$\ln\left(\frac{W_{eq}}{W_{eq} - W}\right) = Kt \quad (13)$$

$$\frac{dW}{dt} = K(W_{eq} - W)^2 \quad (14)$$

$$\frac{t}{W} = \frac{1}{KW_{eq}^2} + \frac{1}{W_{eq}}t \quad (15)$$

The calculated constants adjusted to the second-order kinetics show higher values in intermediate pH values than in the extremes for the redox initiated hydrogel. At the extreme values of pH, the ionic hydrogels behave as non-ionic. In addition to that, the rate in the ion exchange seems to be higher when the hydrogel already has certain amount of electrolytes inside. For the thermal initiated hydrogel, the behavior is the opposite, due to the dissociation degree of the acrylic acid based on the Henderson–Hasselbach relation (Table 2) on which below pH = 4.0, the potential of dissociation is higher compared with pH ≥ 5.0. The values of the constants for the redox initiated (Figure 12a) are two orders of magnitude higher than the thermal (Figure 12b), confirming the high responsive behavior of the redox initiated hydrogel.

The rate of swelling of a hydrogel is controlled by the mesh size (ξ) of the network. The mesh size can be theoretically determined based on the cross-linking density by calculating the distance of the swollen polymer chains between cross-linked points (based on Peppas[50]).

$$\xi = l(\nu_{2eq})^{-1/3} \cdot \sqrt{\frac{C_n}{X}} \quad (16)$$

where *l*, is the bond length along the backbone chain ($1.54\times10^{-10}$ m for carbon-carbon bonds), $v_{2eq}$ is the swollen polymer volume fraction assuming isotropic swelling (xerogel volume/ hydrogel volume in the case of PAA), $C_n$ is the Flory characteristic ratio (for PAA, $C_n = 6.7$)[46] and *X* is the degree of cross-linking (1% molar with respect to monomer concentration).

Figure 13 shows that the mesh size increases at higher pH values, confirming the expansion in the volume of the hydrogel due to swelling and repulsion of carboxylic groups. For the redox initiated, the mesh size is small compared with other works[47,50] giving the possibility of prevent aggregation of NPs which was discussed before. For the thermal initiated

hydrogel, the mesh size varies more, correlating its behavior with the higher swelling capacity. However in the intermediate pH values, the swelling for this hydrogel is similar, showing no change in the mesh size due to the pKa values of the PAA lie between these pH values. In the redox initiated hydrogel, this change cannot be seen because the amount of electrolytes smoothes the transition. A change in the chain length of 2 nm between cross-links can generate a mass gain of 700% the weight of the xerogel for the redox initiated case. A change in 4 nm generates almost 1700% for the thermal initiated hydrogel (Figure 13).

The calculated molecular weight of the polymer chains between cross-linked points $M_c$ is 3603 g/mol using $M_c = M_0/2X$ with $M_0$ as the molecular weight of the repeating units. For these values, the polymer volume fraction $v_{2eq}$ decreases at higher pH values, going from 0.31 to 0.11 for redox and from 0.33 to 0.05 for thermal initiated hydrogel. This confirms the increase in mesh size ξ and hence, the volume of the hydrogel. Due to the presence of electrolytes in the redox hydrogel, its $v_{2eq}$ is higher, which represents lower swelling.

### 3.4 Membrane characterization

Knowing that PAA is present in the interior and surface of the membrane, a pH effect on the water flux due this presence is shown in Figure 14. Due to high swelling at high pH values in the cross-linked PAA, hydrogel mesh size increases along with its total volume and in consequence, membrane pore size would decrease. The linear relationship between applied pressure (Δ$P$) from 1 to 4 bars and flux ($J_v$) illustrates a solid pore PAA functionalization and the change in the permeability of the membranes (slopes in the Figure 14). The losses of PAA due to the low pressure applied are negligible due to the fact that these type of hydrogels has a certain degree of stickiness.[51] In addition, some works report that fracture stresses are reached at 130 bar[52]. Assuming cylindrical pores and unchanged porosity in the PVDF-PAA membranes (uniform cross-linked PAA distribution within pores), effective diameters can be estimated by applying Hagen-Poisseuille's modified equation[25]:

$$\frac{P}{P_0} = \left(\frac{d_p}{d_{p0}}\right)^4 \quad (17)$$

where $P$ is the permeability at different pH values of PVDF-PAA membrane, $P_0$ is the permeability of the bare PVDF membrane to pure water, $d_p$ is the equivalent pore diameter of the PVDF-PAA at defined pH and $d_{p0}$ the diameter of bare PVDF membrane. Taking $d_{p0}$ = 650 nm (manufacturer's data) and a measured $P_0$ = 3800 L/ ($m^2$·h·bar), the calculated values of pore diameter at different pH values showed that pore size is more open at low pH values (Table 2). The differences between these calculations and the observed by SEM (PVDF-PAA = 690 ± 58 nm) are due possibly to that each membrane is dehydrated for sample preparation and thus, the polymer returns to its xerogel size opening the membrane pores. The mesh size values calculated in the hydrogel characterization have an inverse relationship with permeability as expected due swelling of the hydrogel, limiting the flux through the membrane's pores. An increase from 5.89 to 8.33 nm for ξ represents great changes in the hydrogel macrostructure creating almost a 93% of decrease in the permeability of PVDF-PAA membranes from redox initiation (Table 2). This calculated

mesh size is small compared with other works[46,50] giving the advantage of preventing NPs aggregation.

### 3.5 TCE reductive dechlorination

Various literature studies have showed the effect of iron NPs in dechorination processes and why it is advantageous to have the polymer/membrane support for them. Due to the low amount of iron found from polymerization studies, the dechlorination experiments in membranes were compared with and without the ion exchange procedure. For reduction of iron, only $NaBH_4$ was used. The tea extract as reducing agent from a previous works[43] was not used because this extract acts as capping agent too, which makes some of the NPs surface less available for Pd deposition in the post-coating.

After having the functionalized hydrogel and membranes, they were tested to reduce TCE. During the reduction of $Fe^{2+}$ to NPs, the carboxylic groups made a $Na^+$ bond from the $NaBH_4$ used. The addition of Pd to Fe NPs reduces the time of having the same dechlorination yield using Fe NPs alone, because Pd catalyses the production of hydrogen by Fe corrosion.[43] As shown in Figure 15 (hydrogel) and Figure 16 (hydrogel in membrane), the reduction of TCE is confirmed by the reduction of its concentration as well the increase in the chloride concentration with time (Figure 15). $[Cl^-]_{MAX}$ indicates the maximum possible amount of chloride that can be formed based in the TCE loaded at the beginning of the process. Comparing with other solution phase (not immobilized iron) studies that used CMC to prevent aggregation,[53] it can be established that PAA based immobilization systems also prevents NPs aggregation and provides high dechlorination rates. In addition to that, hydrogel and membrane behaviors showed an increase in the reactivity by the increasing in Fe loading, which is confirmed by other studies.[25] The loss of iron for hydrogel/membrane systems was 0.1%, and for hydrogel, 0.5% weight during the reductive dechlorination experiments. The amount of Pd coating was not analyzed directly, but it affects the reaction rate depending on the extent of coverage of reactive by Pd layers on the Fe surface.[42]

The batch reduction with metal (Fe/Pd) NPs will follow a pseudo-first order reaction kinetics:[54]

$$-\frac{dC}{dt}=k_{obs}C=k_{sa}a_s\rho_m C \quad (18)$$

where $k_{obs}$ is the observed pseudo-first order rate constant ($h^{-1}$), $C$ is the TCE concentration (mg/L) at time $t$ (h), $k_{sa}$ is the surface-area rate constant normalized with respect to particle size ($L/m^2{\cdot}h$), $a_s$ is the specific surface area of the NPs determined before (12.7 $m^2/g$) and $\rho_m$ is the NPs loading (g/L). The $k_{sa}$ values for each system are reported in the Figure 15 and Figure 16 for hydrogel and membranes, respectively. The $k_{sa}$ value for the hydrogel system is higher than for the membranes due to a more open area and larger volume for reaction. A comparison between the performance of these membranes and other works from our group show similar $k_{sa}$ values using $NaBH_4$ as reducing agent: Smuleac[43] reported a $k_{sa}$ of 0.105 $L/m^2h$ for a similar Pd coating (3.0%) while Xu,[42] reported a $k_{sa}$ of 0.068 $L/m^2h$ with lower Pd coating (2.3%). These results demonstrate that the redox functionalization of the membrane give comparable results and can be used as an alternative in dechlorination

processes. On the other hand, the membrane used directly from the redox polymerization avoiding ion exchange had very low iron concentration and this value is near to the error range reported from atomic absorption analysis. This result implies that almost no reaction was achieved or there is a need of longer times to determine the rate constant.

In Figure 17, the molar ratio between chloride formation and TCE degradation is slightly lower (≈10%) than the stoichiometric 3:1 (dash line). This confirms the dechlorination of the pollutant without formation of byproducts, which is the main purpose of using Fe/Pd NPs. Although the maximum amount of iron in the membranes is near the calculated value, the reactivity in membrane domain is lower compared with the hydrogel alone. This is explained by the limitations in the diffusion and convective processes due to the performance of the batch experiment.

## 4. Conclusions

This study demonstrates that the synthesis of 60 nm Fe NPs in PAA hydrogel and membranes using the metal accelerant from the PAA hydrogel redox polymerization is feasible. NPs formed in the macro-structure of the hydrogel showed low aggregation demonstrating the immobilization in different platforms (hydrogel/membrane).

The PAA hydrogel formed can be used alone directly in catalytic processes after polymerization, avoiding ion exchange processes. After ion exchange, the PAA hydrogel showed a large iron loading capacity, allowing less polymer material in the reaction system. This feature can be applied in direct injection for underground water treatment.

It was demonstrated a relationship between the mesh size of the hydrogel and the pore size of the membrane due to pH changes by swelling and permeability measurements. Mesh size dependence of pH variations in the hydrogel is an important factor in the ion exchange processes towards higher Fe loading.

The dechlorination of TCE was performed by Fe/Pd NPs in both hydrogel/membrane and single hydrogel systems, showing direct dependence on the Fe amount (and Pd coating). The produced chloride using bimetallic Fe/Pd nanoparticles in dechlorination experiments is close to the stoichiometric value, indicating negligible production of intermediates. Rate constants of dechlorination have similar values than previous works demonstrating the effectiveness of the functionalization based on redox polymerization.

## Acknowledgments

This study was supported by the National Institute of Environmental Health Sciences/National Institutes of Health Superfund (NIEHS-SRP) program. J. K. Papp, was supported by the NSF-REU program too. This group thanks the Electron Microscopy Center (University of Kentucky) and the Environmental Research and Training Laboratory (University of Kentucky).

## References

1. Bruening M, Dotzauer D, Jain P, Ouyang L, Baker G. Creation of functional membranes using polyelectrolyte multilayers and polymer brushes. Langmuir : the ACS journal of surfaces and colloids. 2008; 24:7663–7673. [PubMed: 18507420]

2. Sudipta S, Guibal E, Quignard F, SenGupta AK. Polymer-supported metals and metal oxide nanoparticles: synthesis, characterization, and applications. J Nanopart Res. 2012; 14
3. Andrij ZP, Hans-Juergen PA. Composite aqueous microgels: an overview of recent advances in synthesis, characterization and application. Polym Int. 2007; 56
4. Yan L, Paul S, Yu M, Matthias B, Andrij P. Composite Hydrogels: Robust Carriers for Catalytic Nanoparticles. Macromol Chem Phys. 2007; 208
5. Nagaraja GK, Demappa T, Mahadevaiah. Polymerization kinetics of acrylonitrile by oxidation: Reduction system using potassium persulfate/ascorbic acid in an aqueous medium. J Appl Polym Sci. 2011; 121
6. Braun, D. Polymer synthesis : theory and practice : fundamentals, methods, experiments. Berlin; New York: Springer; 2005.
7. Kricheldorf, HR. Handbook of polymer synthesis. New York: Marcel Dekker; 2004.
8. Odian, G. Principles of polymerization. New York; Chichester: Wiley; 2004.
9. Sarac AS. Redox polymerization. Prog Polym Sci. 1999; 24:1149–1204.
10. Hsieh Y, Hsieh Y. Valence State of Iron in the Presence of Ascorbic Acid and Ethylenediaminetetraacetic Acid. J Agr Food Chem. 1997
11. Khan M, Martell A. Metal ion and metal chelate catalyzed oxidation of ascorbic acid by molecular oxygen. I. Cupric and ferric ion catalyzed oxidation. J Am Chem Soc. 1967; 89:4176–4185. [PubMed: 6045609]
12. Liang CJ, Bruell CJ, Marley MC, Sperry KL. Persulfate oxidation for in situ remediation of TCE. II. Activated by chelated ferrous ion. Chemosphere. 2004; 55:1225–1233. [PubMed: 15081763]
13. He F, Zhao DY, Liu JC, Roberts CB. Stabilization of Fe-Pd nanoparticles with sodium carboxymethyl cellulose for enhanced transport and dechlorination of trichloroethylene in soil and groundwater. Ind Eng Chem Res. 2007; 46:29–34.
14. Meng ZH, Liu HL, Liu Y, Zhang J, Yu SL, Cui FY, Ren NQ, Ma J. Preparation and characterization of Pd/Fe bimetallic nanoparticles immobilized in PVDF.Al2O3 membrane for dechlorination of monochloroacetic acid. J Membrane Sci. 2011; 372:165–171.
15. Lewis, SR.; Smuleac, V.; Xiao, L.; Bhattacharyya, D. Responsive Membranes and Materials. John Wiley & Sons, Ltd.; 2012. Tunable Separations, Reactions, and Nanoparticle Synthesis in Functionalized Membranes; p. 97-142.
16. Thomas V, Namdeo M, Murali Mohan Y, Bajpai SK, Bajpai M. Review on Polymer, Hydrogel and Microgel Metal Nanocomposites: A Facile Nanotechnological Approach. Journal of Macromolecular Science, Part A. 2007; 45:107–119.
17. Xu J, Dozier A, Bhattacharyya D. Synthesis of nanoscale bimetallic particles in polyelectrolyte membrane matrix for reductive transformation of halogenated organic compounds. J Nanopart Res. 2005; 7:449–467.
18. Zhang J, Xu S, Kumacheva E. Polymer Microgels: Reactors for Semiconductor, Metal, and Magnetic Nanoparticles. J Am Chem Soc. 2004; 126:7908–7914. [PubMed: 15212539]
19. Sahiner N, Butun S, Ozay O, Dibek B. Utilization of Smart Hydrogel-Metal Composites as Catalysis Media. J Colloid Interf Sci. 2012; 373:122–128.
20. Carotenuto G, Martorana B, Perlo PB, Nicolais L. A universal method for the synthesis of metal and metal sulfide clusters embedded in polymer matrices. J Mater Chem. 2003; 13:2927–2930.
21. Wu W, He QG, Jiang CZ. Magnetic Iron Oxide Nanoparticles: Synthesis and Surface Functionalization Strategies. Nanoscale Res Lett. 2008; 3:397–415. [PubMed: 21749733]
22. Carotenuto G, DeNicola S, Pepe GP, Nicolais L. A qualitative model for the growth mechanism of silver clusters in polymer solution. Eur Phys J B. 2001; 24:437–441.
23. Patrick S, Gudrun S. Nanocomposite polymer hydrogels. Colloid Polym Sci. 2008; 287
24. Ulbricht M. Advanced functional polymer membranes. Polymer. 2006
25. Smuleac V, Bachas L, Bhattacharyya D. Aqueous - Phase Synthesis of PAA in PVDF Membrane Pores for Nanoparticle Synthesis and Dichlorobiphenyl Degradation. J Memb Sci. 2010; 346:310–317. [PubMed: 20161475]
26. Hu K, Dickson JM. Development and characterization of poly(vinylidene fluoride)–poly(acrylic acid) pore-filled pH-sensitive membranes. J Membrane Sci. 2007; 301:19–28.

27. Yian Z, Wenbo W, Gong Z, Aiqin W. Enhanced Selectivity for Heavy Metals Using Polyaniline-Modified Hydrogel. Ind Eng Chem Res. 2013; 52
28. Minghui G, Lindell EO, Dibakar B. Reactive Functionalized Membranes for Polychlorinated Biphenyl Degradation. Ind Eng Chem Res. 2013; 52
29. Yuvakkumar R, Elango V, Rajendran V, Kannan N. Preparation and Characterization of Zero Valent Iron Nanoparticles. Dig J Nanomater Bios. 2011; 6:1771–1776.
30. Misra GS, Bajpai UDN. Redox polymerization. Prog Polym Sci. 1982; 8:61–131.
31. Fordham JWL, Williams HL. Journal of the American Chemical Society- 1951 - Fordham, Williams.pdf. J Am Chem Soc. 1951; 73:4855–4859.
32. Gibbs MM. A simple method for the rapid determination of iron in natural waters. Water Res. 1979; 13:295–297.
33. Stookey LL. Ferrozine - a New Spectrophotometric Reagent for Iron. Anal Chem. 1970; 42:779.
34. José RQ, Nora EV, Issa K. Synthesis and Swelling Kinetics of Poly(Dimethylaminoethyl acrylate methyl chloride quaternary- co -itaconic acid) Hydrogels. Langmuir. 1999; 15
35. Cutie SS, Smith PB, Henton DE, Staples TL, Powell C. Acrylic acid polymerization kinetics. J Polym Sci Pol Phys. 1997; 35:2029–2047.
36. Sun XL, Sun HH, Wang YA. Polyacrylamide Gel Polymerization: Ascorbic Acid-ferrous Sulfate-ammonium Persulfate Initiator for Acid System. Sheng wu hua xue yu sheng wu wu li xue bao Acta biochimica et biophysica Sinica. 1998; 30:407–410.
37. Manickam SP, Venkatarao K, Subbaratnam NR. Peroxo salts as initiators of vinyl polymerization —2. Kinetics of polymerization of acrylic acid and sodium-acrylate by peroxodisulphate in aqueous solution—effect of pH and Ag+ catalysis. Eur Polym J. 1979; 15
38. Kabanov V, Topchiev D, Karaputadze T, Mkrtchian L. Kinetics and mechanism of radical polymerization of weak unsaturated acids in aqueous solutions. Eur Polym J. 1975
39. Glavee GN, Klabunde KJ, Sorensen CM, Hadjipanayis GC. Chemistry of Borohydride Reduction of Iron(II) and Iron(III) Ions in Aqueous and Nonaqueous Media. Formation of Nanoscale Fe, FeB, and Fe2B Powders. Inorganic Chemistry. 1995; 34:28–35.
40. He F, Zhao DY. Hydrodechlorination of trichloroethene using stabilized Fe- Pd nanoparticles: Reaction mechanism and effects of stabilizers, catalysts and reaction conditions. Appl Catal B-Environ. 2008; 84:533–540.
41. Sun Y-P, Li X-q, Cao J, Zhang W-x, Wang H. Characterization of zerovalent iron nanoparticles. Adv Colloid Interfac. 2006; 120:47–56.
42. Xu J, Bhattacharyya D. Fe/Pd nanoparticle immobilization in microfiltration membrane pores: Synthesis, characterization, and application in the dechlorination of polychlorinated biphenyls. Ind Eng Chem Res. 2007; 46:2348–2359.
43. Smuleac V, Varma R, Sikdar S, Bhattacharyya D. Green Synthesis of Fe and Fe/Pd Bimetallic Nanoparticles in Membranes for Reductive Degradation of Chlorinated Organics. J Membrane Sci. 2011; 379:131–137.
44. Chen J, Hamon MA, Hu H, Chen Y, Rao AM, Eklund PC, Haddon RC. Solution properties of single-walled carbon nanotubes. Science. 1998; 282:95–98. [PubMed: 9756485]
45. Cohen-Ofri I, Weiner L, Boaretto E, Mintz G, Weiner S. Modern and fossil charcoal: aspects of structure and diagenesis. Journal of Archaeological Science. 2006; 33:428–439.
46. Thakur A, Wanchoo R, Singh P. Structural parameters and swelling behavior of pH sensitive poly (acrylamide-co-acrylic acid) hydrogels. Chem Biochem Eng Q. 2011; 25:181–194.
47. Pa Achia S, Florea CB. POLY (VINYL ALCOHOL) HYDROGELS INTERACTIONS WITH ELECTROLYTES IN AQUEOUS SOLUTION. Revue Roumaine de Chimie. 2007; 52:1145–1149.
48. Fumio U, Hiroshi Y, Kumiko N, Sachihiko N, Kenji S, Yasunori M. Swelling and mechanical properties of poly(vinyl alcohol) hydrogels. Int J Pharmaceut. 1990
49. Katime I, Velada JL, Novoa R, Apodaca EDd, Puig J, Mendizabal E. Swelling Kinetics of Poly(acrylamide)/Poly(mono-n-alkyl itaconates) Hydrogels. Polym Int. 1996; 40
50. Peppas N, Wright S. Solute Diffusion in Poly(vinyl alcohol)/Poly(acrylic acid) Interpenetrating Networks. Macromolecules. 1996

51. Li W, Zhao H, Teasdale PR, John R, Zhang S. Synthesis and characterisation of a polyacrylamide–polyacrylic acid copolymer hydrogel for environmental analysis of Cu and Cd. Reactive and Functional Polymers. 2002; 52

52. Charles WP, Jonathan JW, Gudrun S. A review on tough and sticky hydrogels. Colloid Polym Sci. 2013; 291

53. Feng H, Dongye Z, Juncheng L, Christopher BR. Stabilization of Fe−Pd Nanoparticles with Sodium Carboxymethyl Cellulose for Enhanced Transport and Dechlorination of Trichloroethylene in Soil and Groundwater. Ind Eng Chem Res. 2007; 46

54. Ebert M, Köber R, Parbs A, Plagentz V, Schäfer D, Dahmke A. Assessing degradation rates of chlorinated ethylenes in column experiments with commercial iron materials used in permeable reactive barriers. Environ Sci Technol. 2006; 40:2004–2010. [PubMed: 16570628]

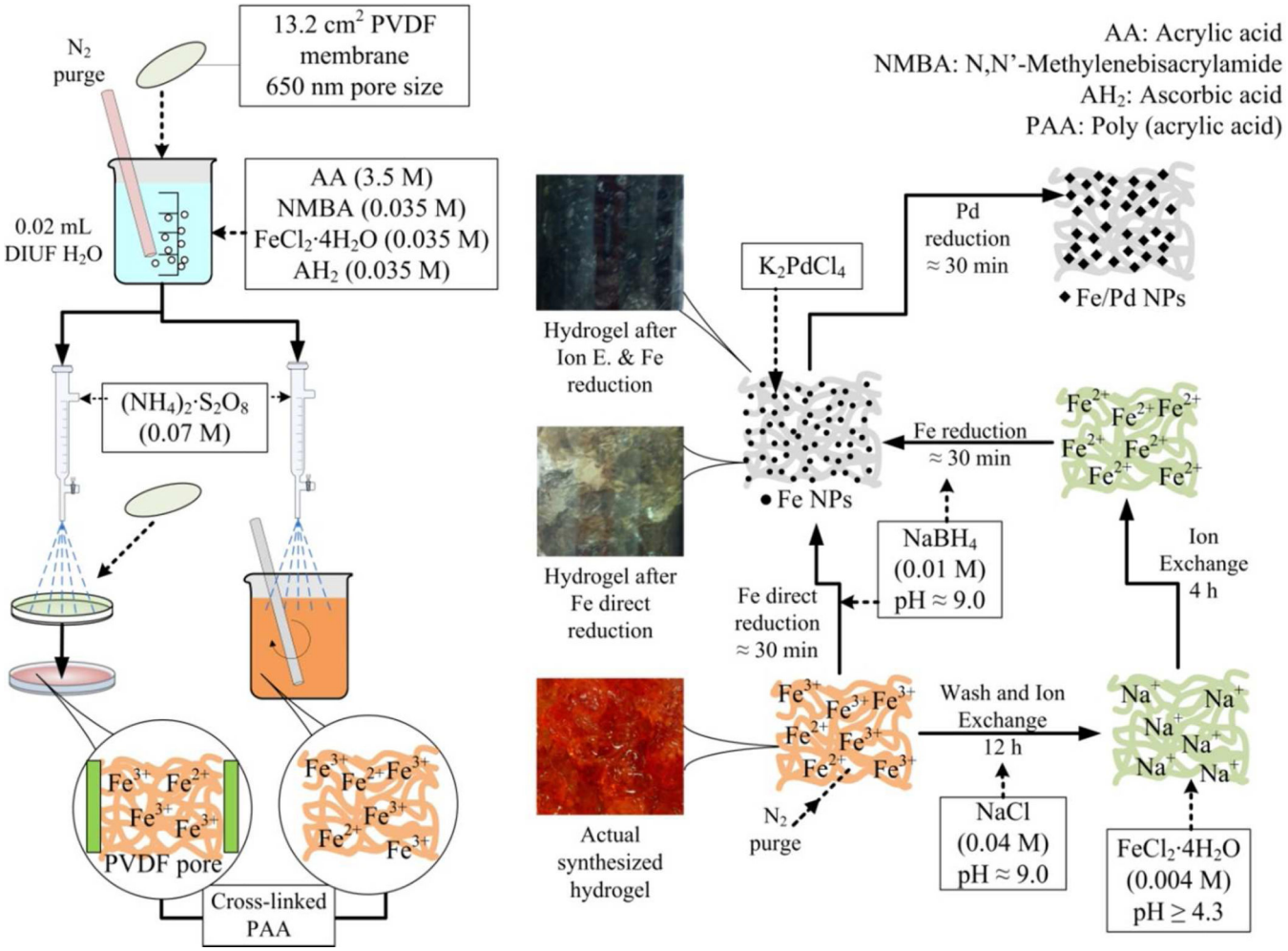


**Figure 1.**

PAA-Hydrogel synthesis and functionalization of PVDF membrane (DVPP Millipore 650 nm pore size, 125 μm thickness, 13.2 $cm^2$ external area) by a redox polymerization of AA and NMBA. For hydrogel synthesis only no PVDF membrane was used.

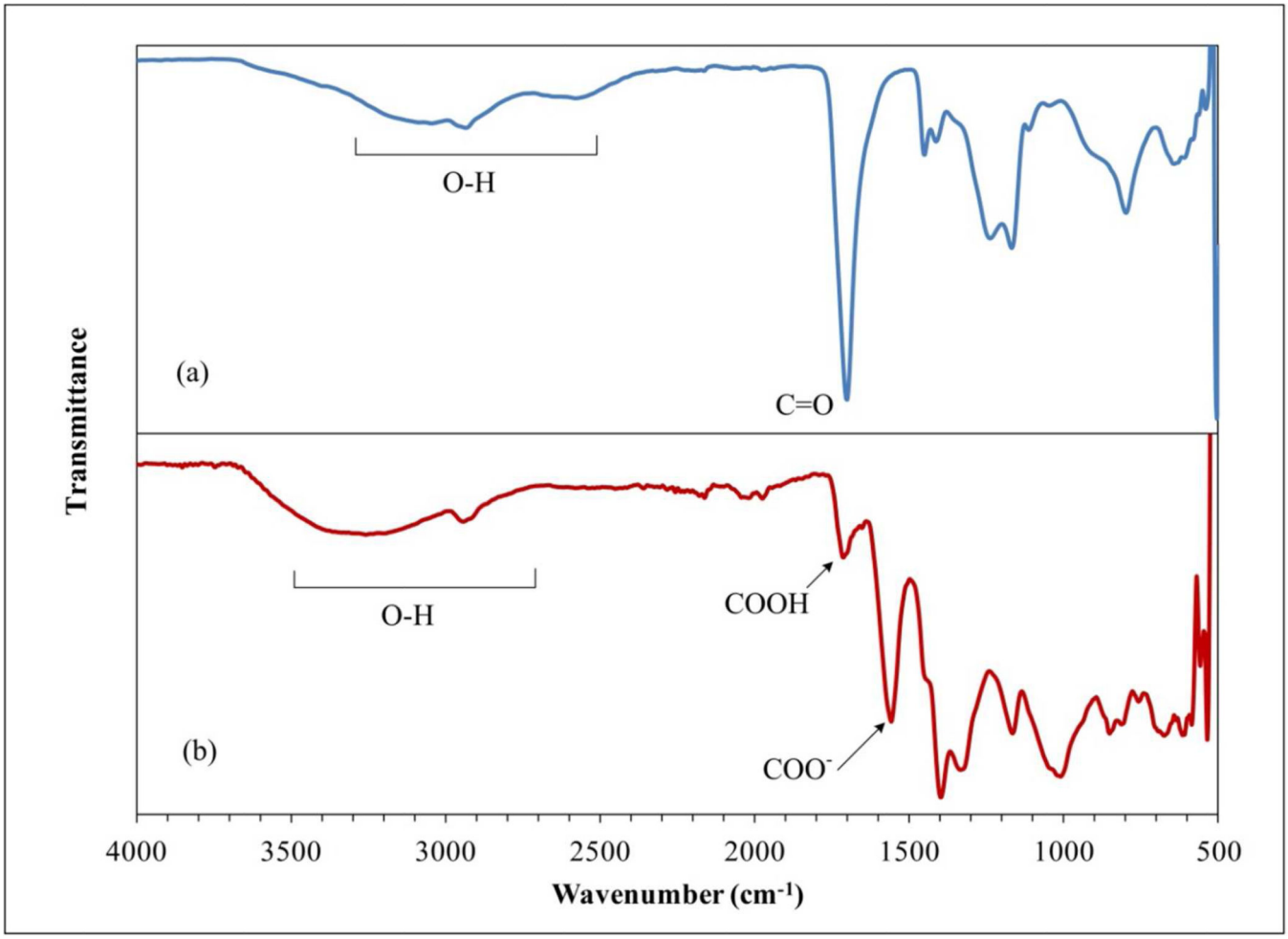


**Figure 2.**
FTIR spectra of (a) PAA powder; (b) PAA cross-linked hydrogel.

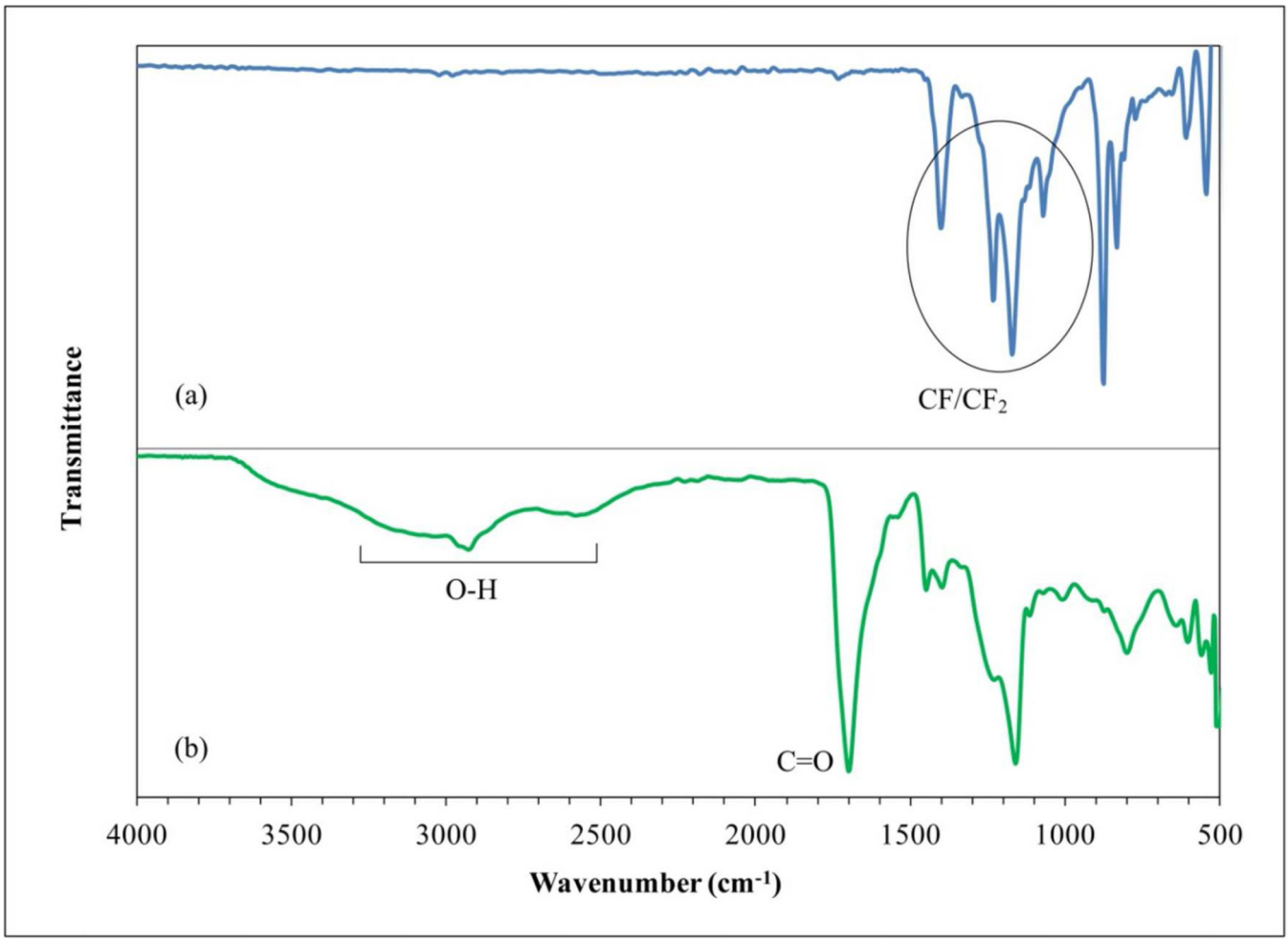


**Figure 3.**
ATR-FTIR spectra of membranes. (a) PVDF membrane; (b) PVDF-PAA membrane.

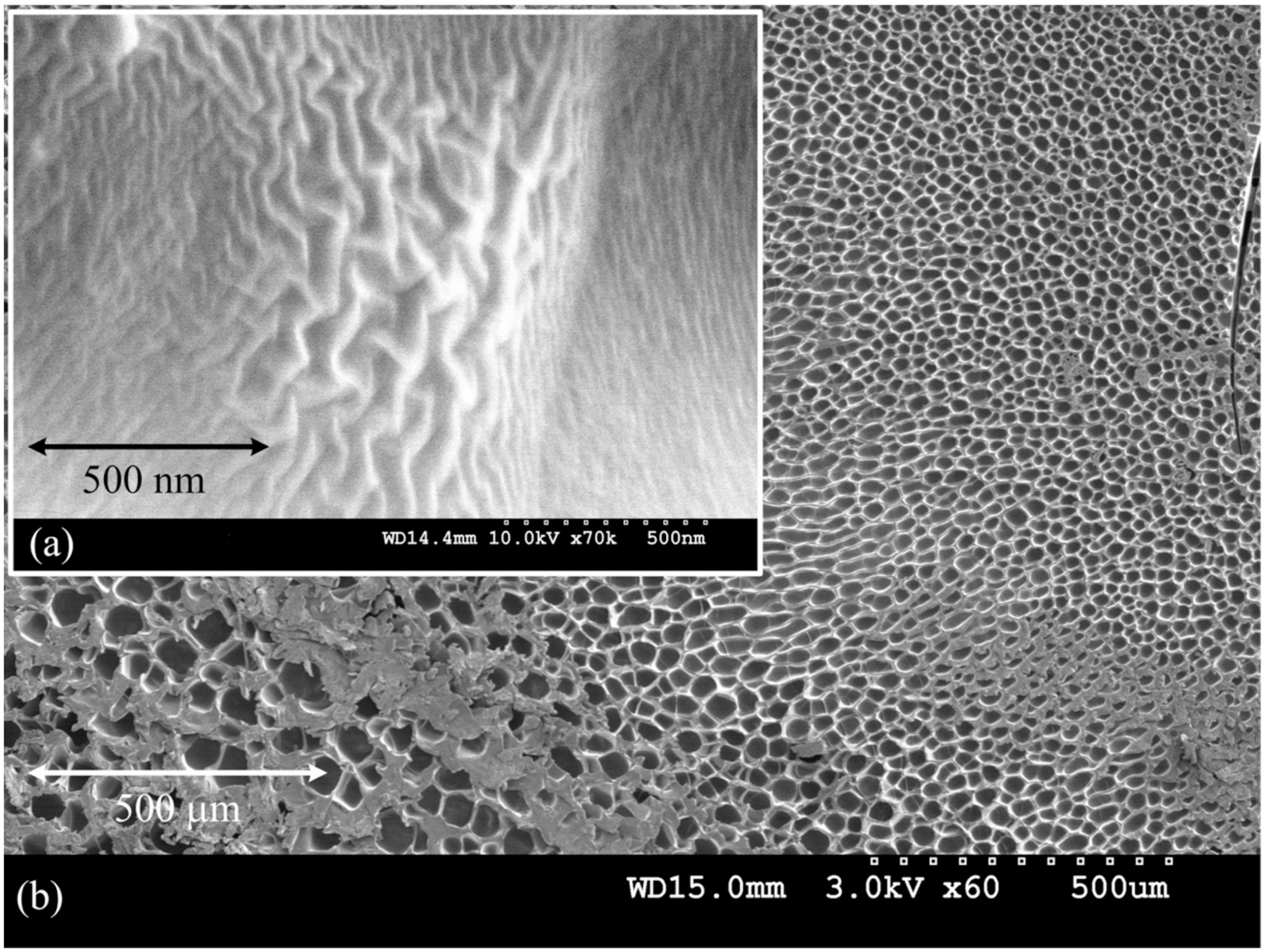


**Figure 4.**
SEM images of the cross-linked PAA-NMBA xerogel. (a) Wrinkled structure of the xerogel, (b) Porous surface of the xerogel.

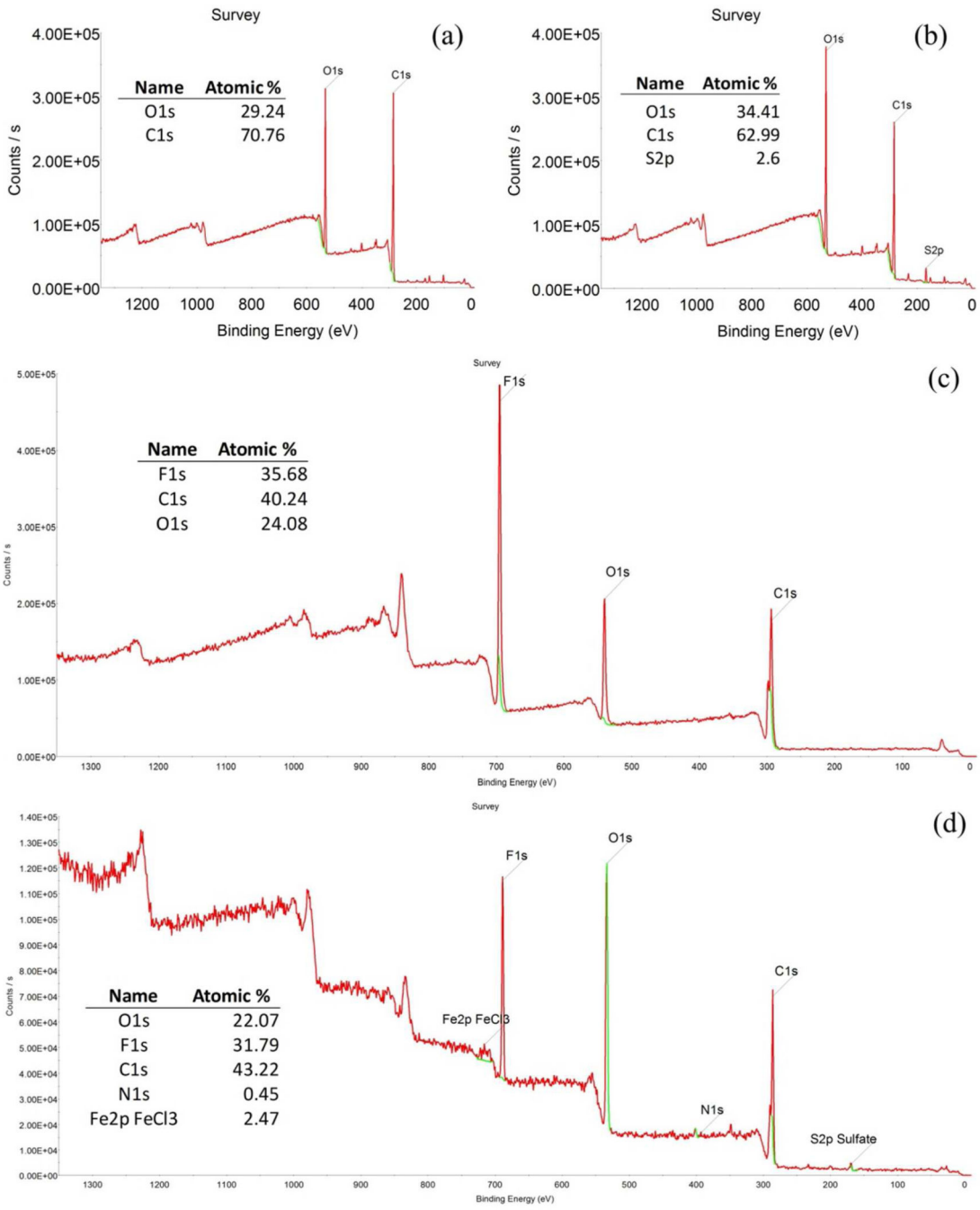


**Figure 5.**

XPS spectrums of the cross-linked PAA xerogel and PVDF-PAA membranes. (a) PAA Xerogel from thermal initiation, (b) PAA Xerogel from redox initiation, (c) PVDF-PAA from thermal initiation, (d) PVDF-PAA from redox initiation.

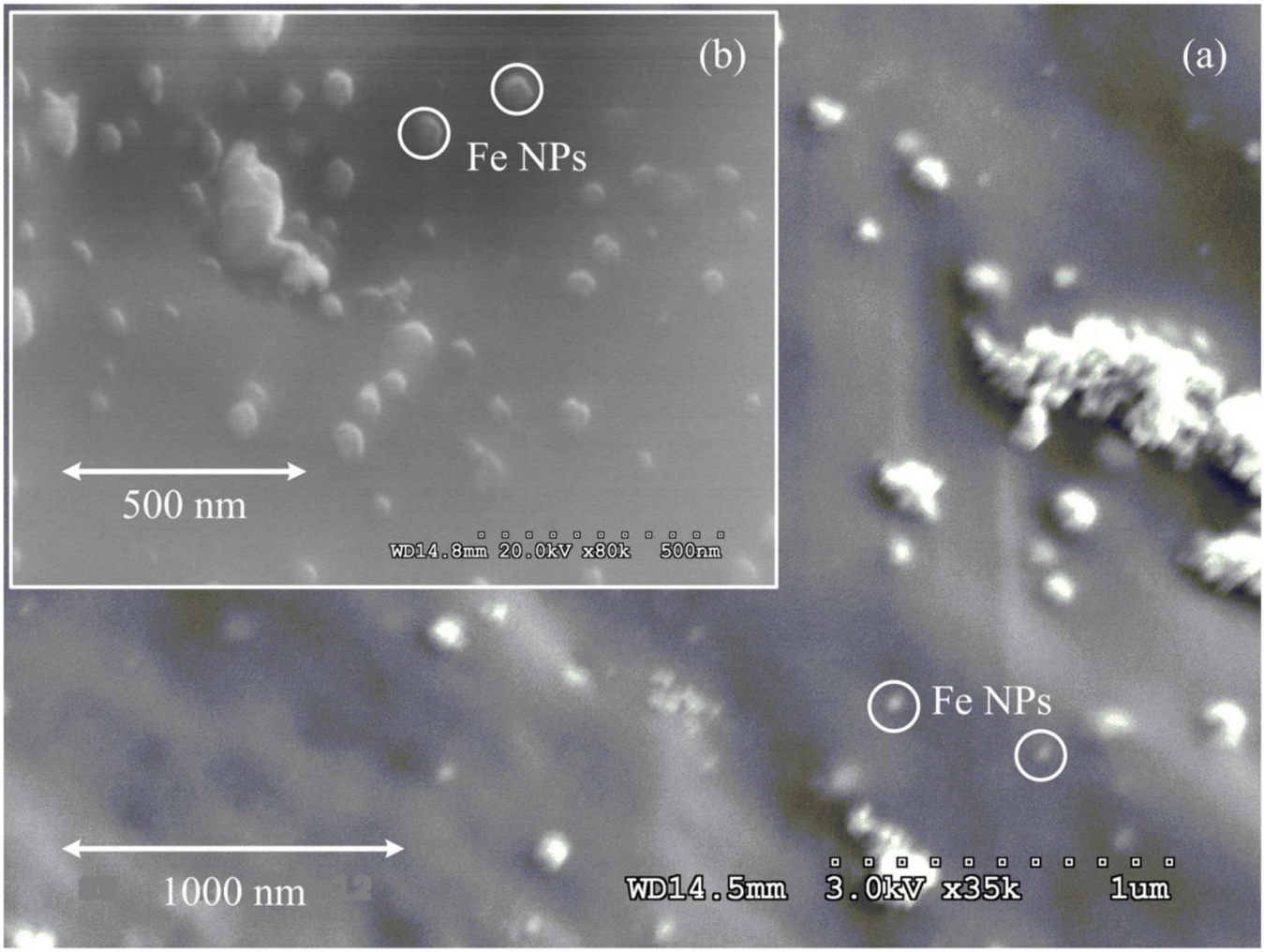


**Figure 6.**
SEM images of the cross-linked PAA-NMBA-Fe xerogel. (a) Pore surface of the xerogel, (b) Surface of the xerogel.

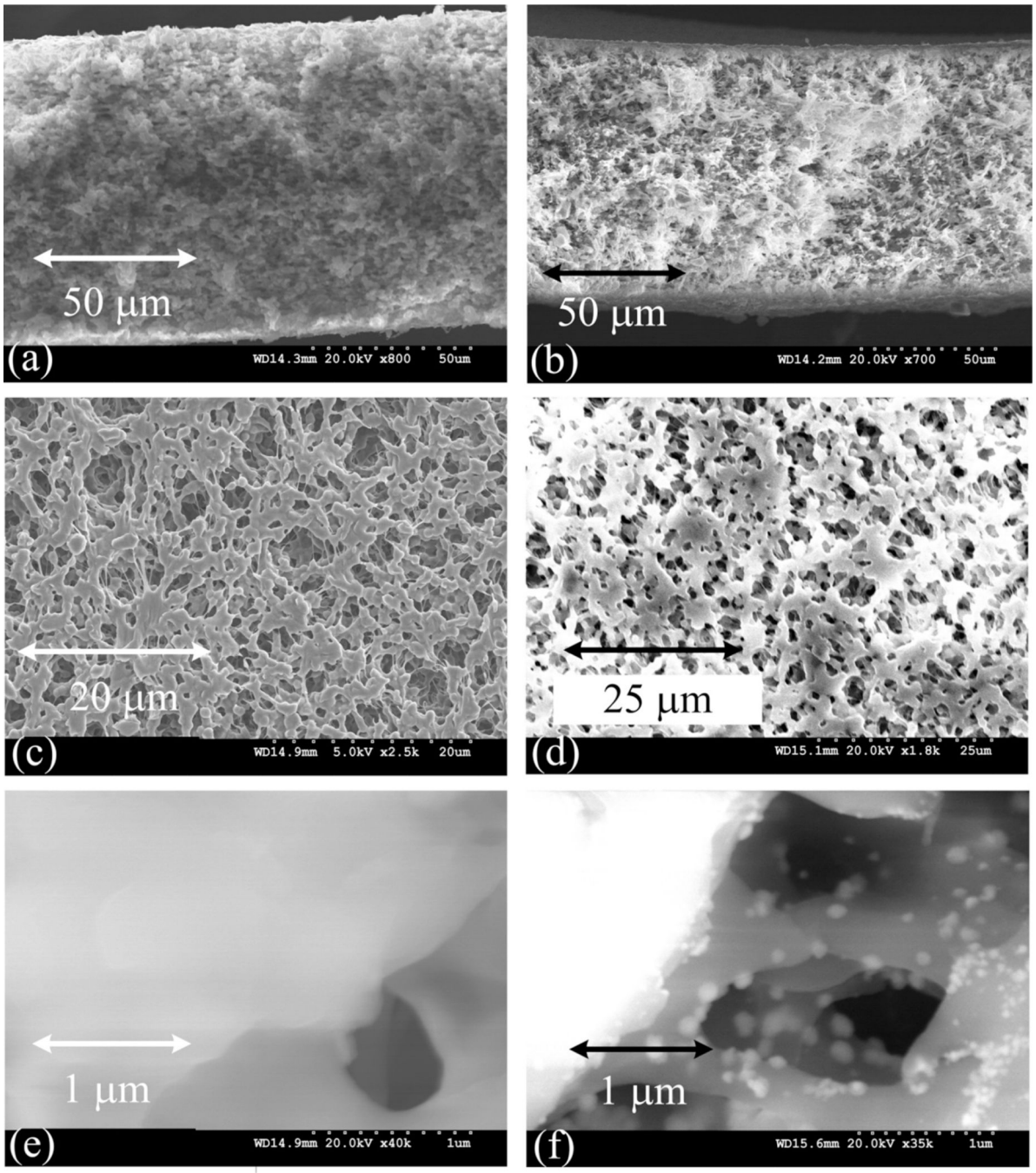


**Figure 7.**

SEM images of bare PVDF, PVDF-PAA and PVDF-PAA-Fe membranes (Millipore). (a) Cross section bare PVDF, (b) Cross section PVDF-PAA, (c) Porous surface PVDF-PAA, (d) Porous surface PVDF-PAA-Fe.

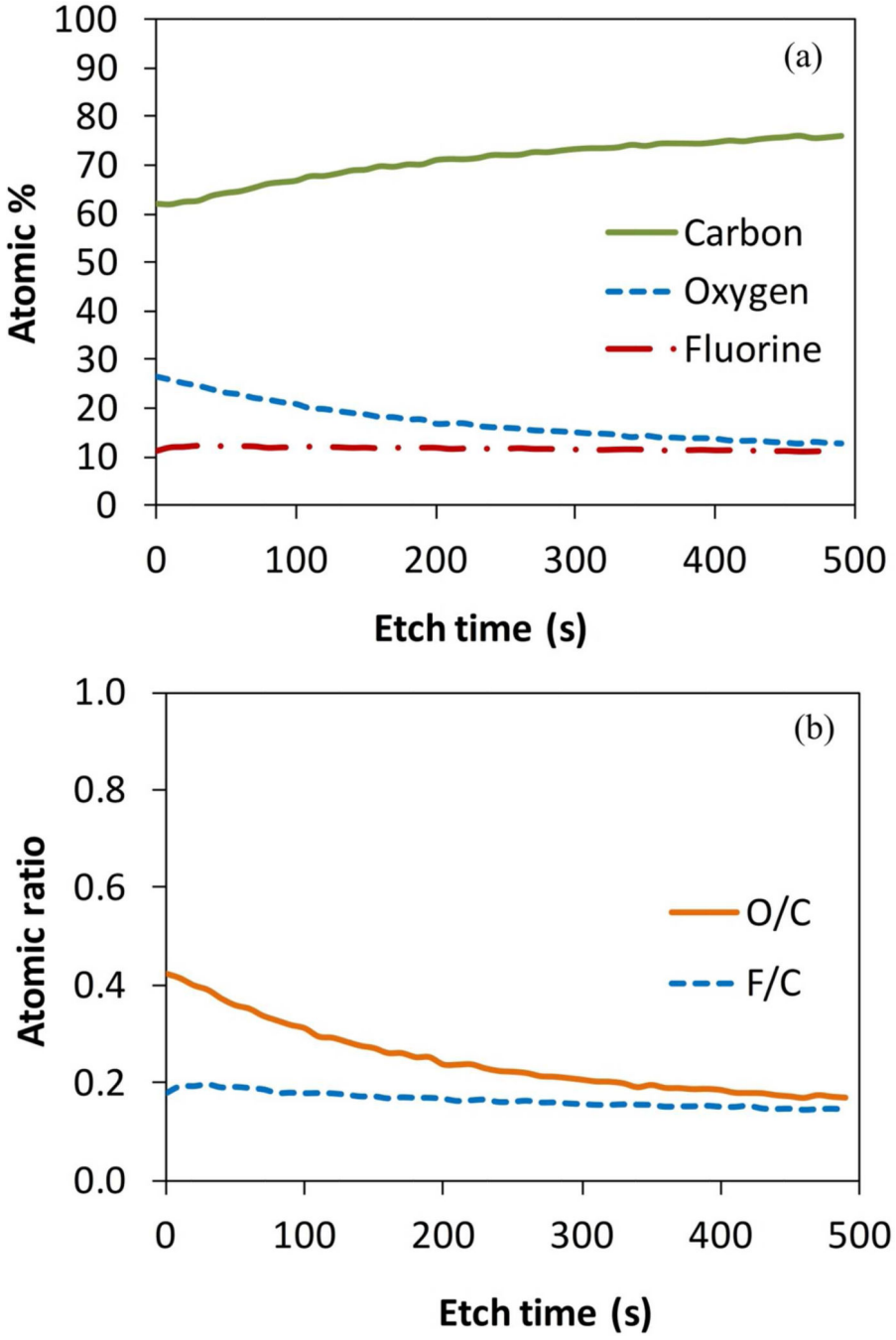


**Figure 8.**
XPS etching in PVDF-PAA membranes (Millipore) by redox polymerization. (a) Atomic percentage composition, (b) Atomic ratio based on carbon element.

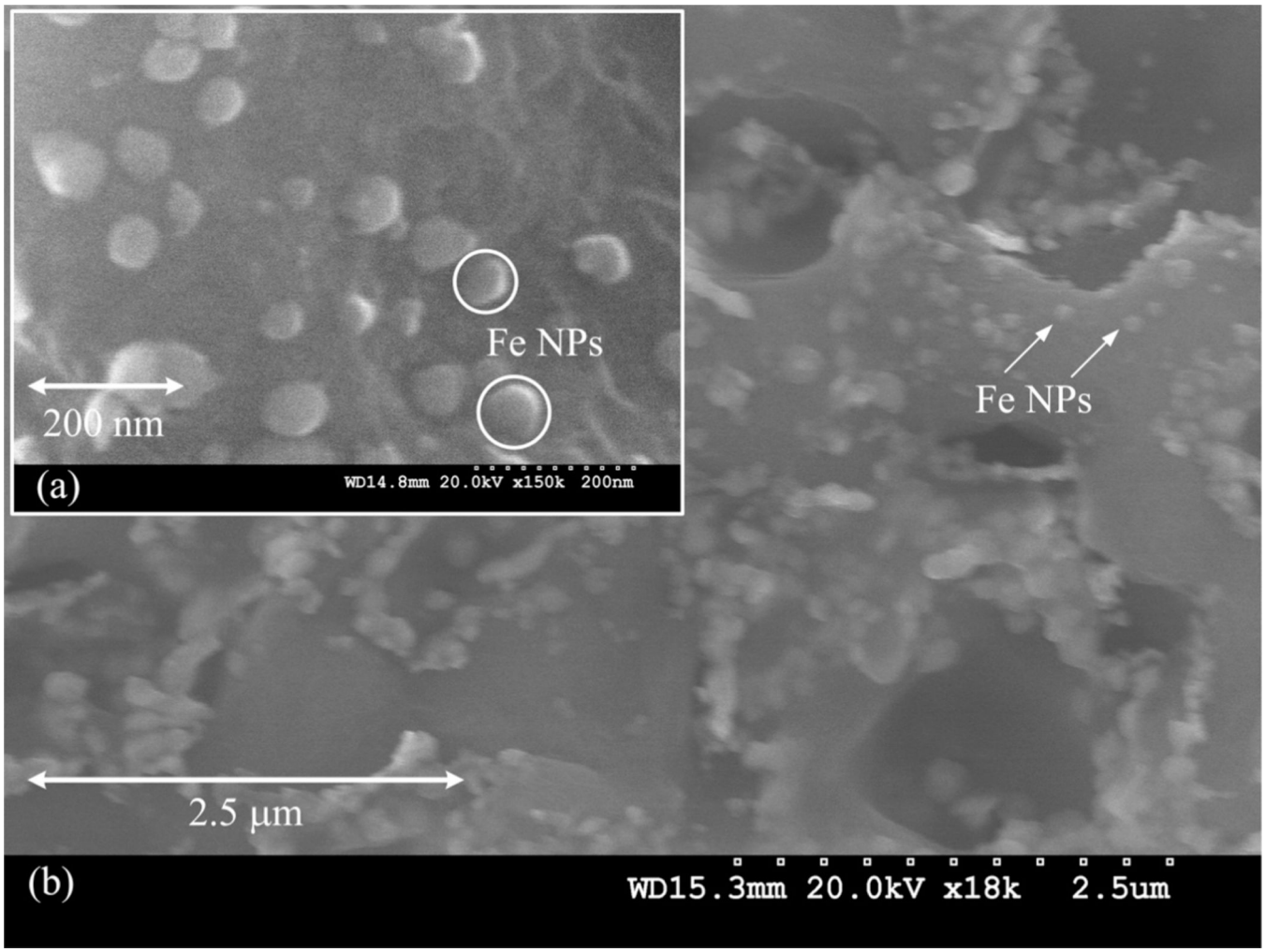


**Figure 9.**
SEM images of PVDF-PAA-Fe membranes (Millipore). (a) Membrane surface, (b) Cross section.

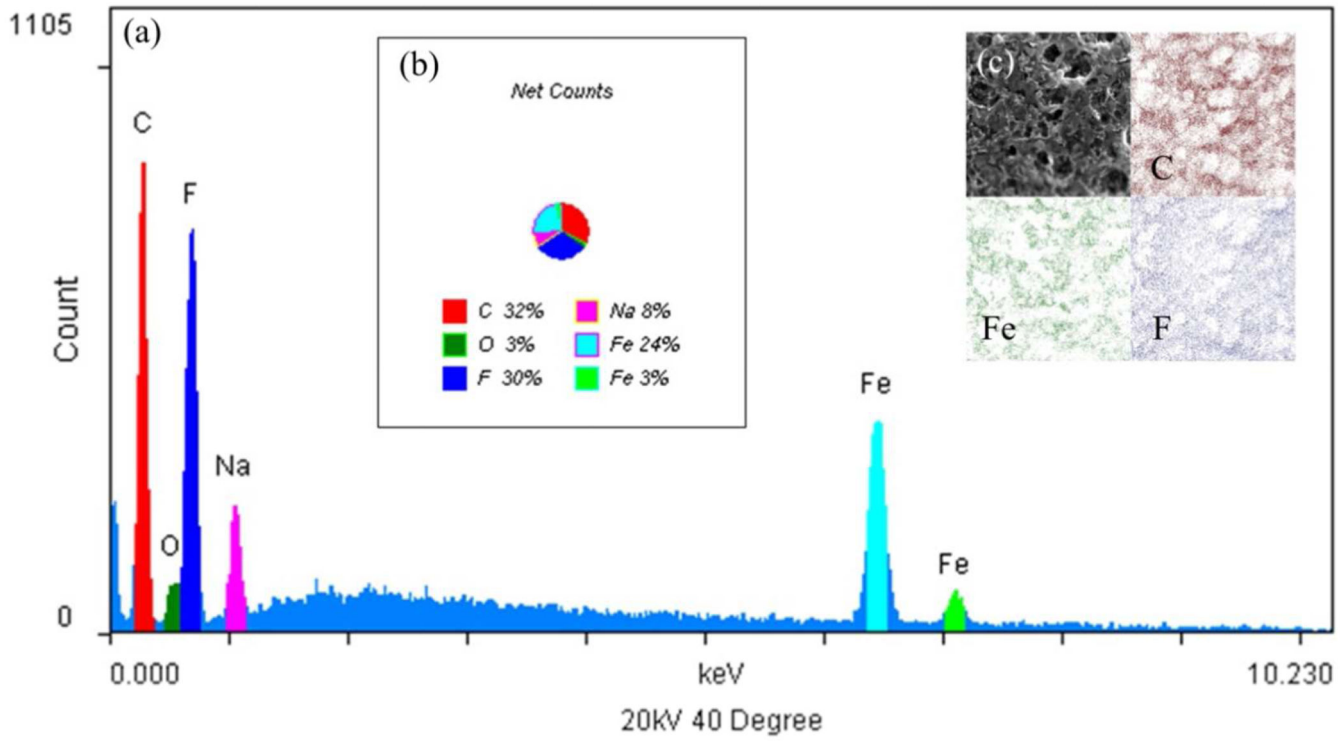


**Figure 10.**

SEM-EDS spectrum and images of PVDF-PAA-Fe membranes (Millipore). (a) EDS spectrum, (b) Elemental net counts, (c) EDS mapping.

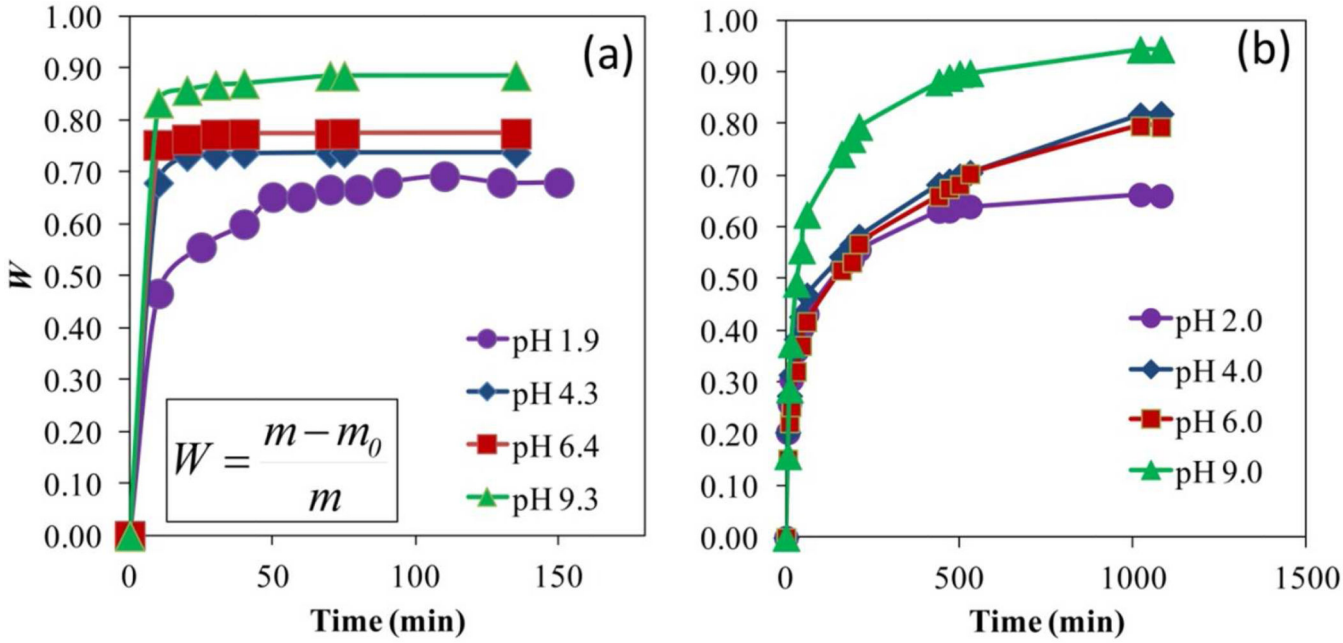


**Figure 11.**

Swelling isotherms of cross-linked PAA hydrogel at different pH values. (a) hydrogel by redox initiation, (b) hydrogel by thermal initiation. Cross-linking, *X* = 1% NMBA. T = 22 °C.

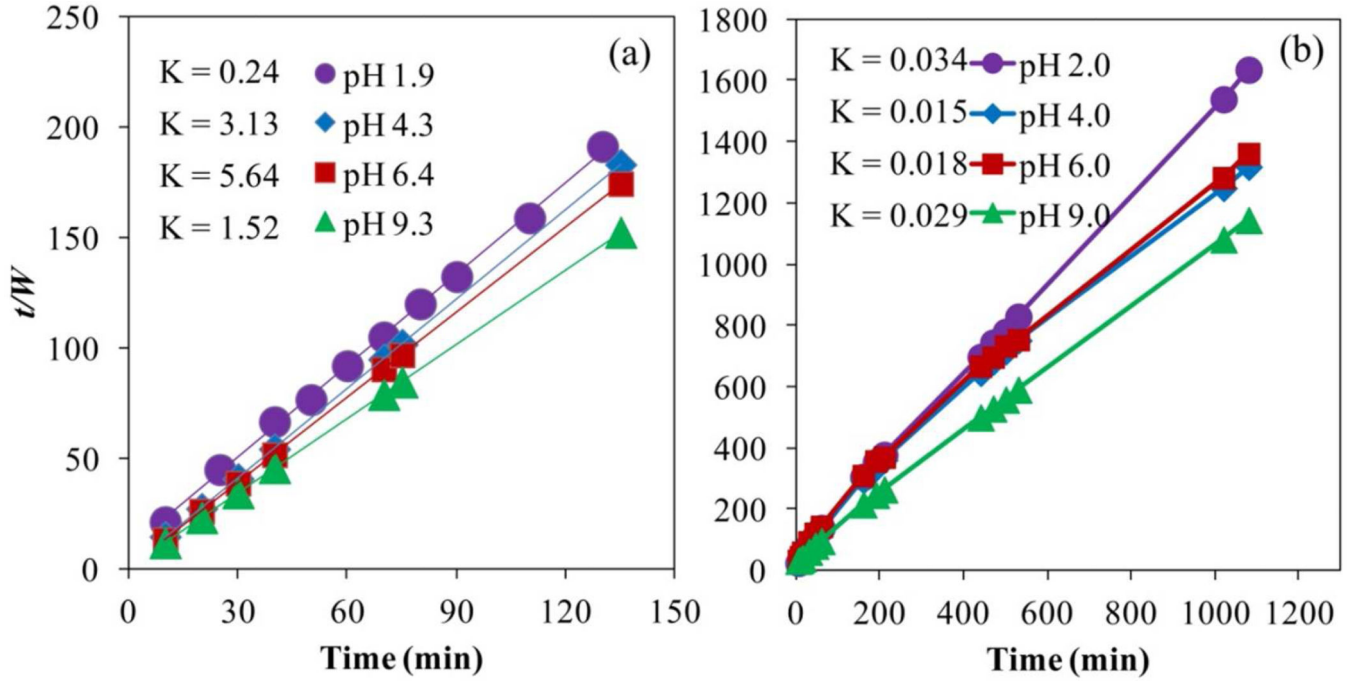


**Figure 12.**

Second-order kinetics model for cross-linked PAA hydrogel at different pH values. (a) hydrogel by redox initiation, (b) hydrogel by thermal initiation. Cross-linking, $X$ = 1% NMBA. T = 22°C.

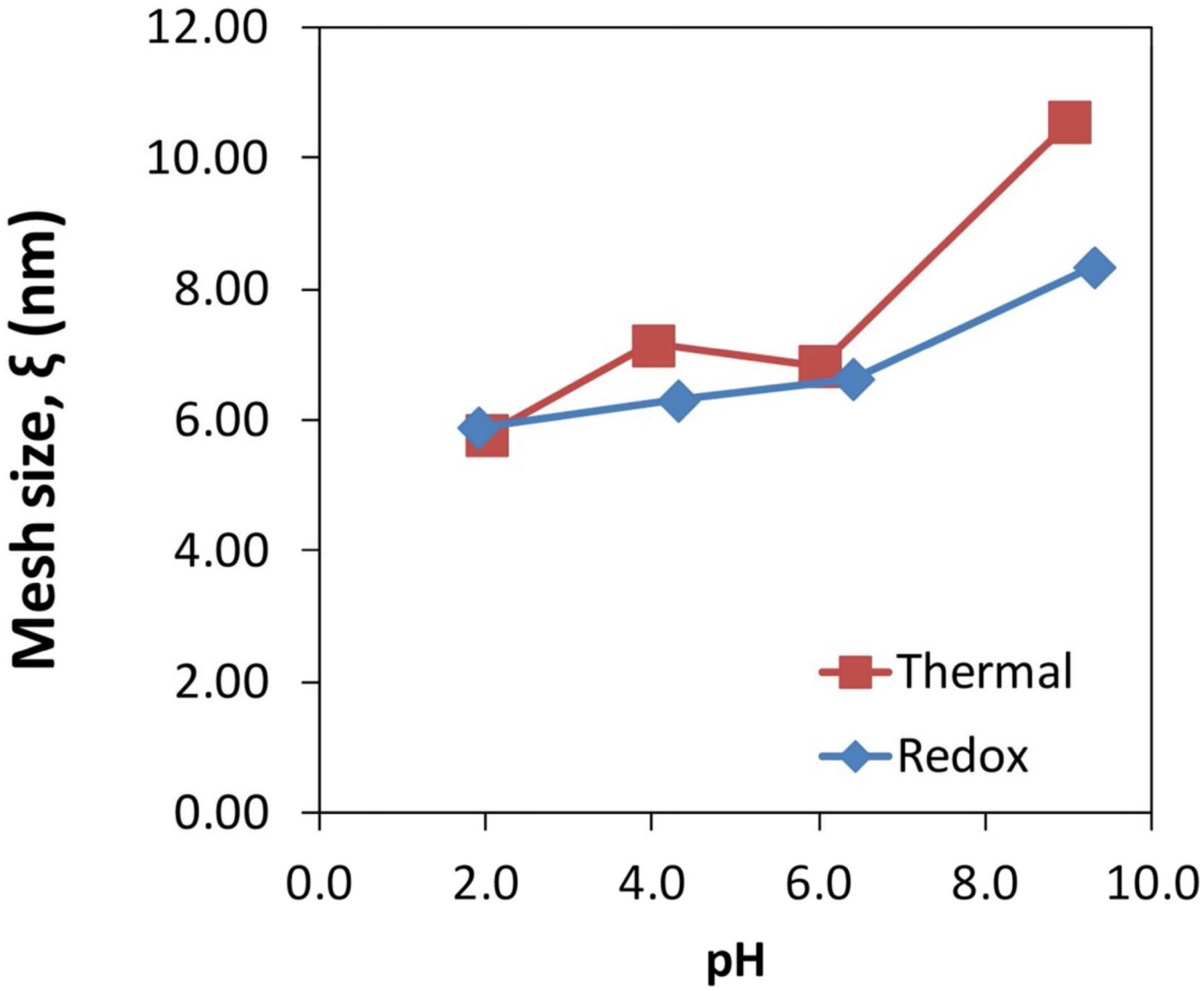


**Figure 13.**
Calculated swollen polymer volume fraction and mesh size of the hydrogel as function of pH. Cross-linking, *X* = 1% NMBA. T = 22°C.

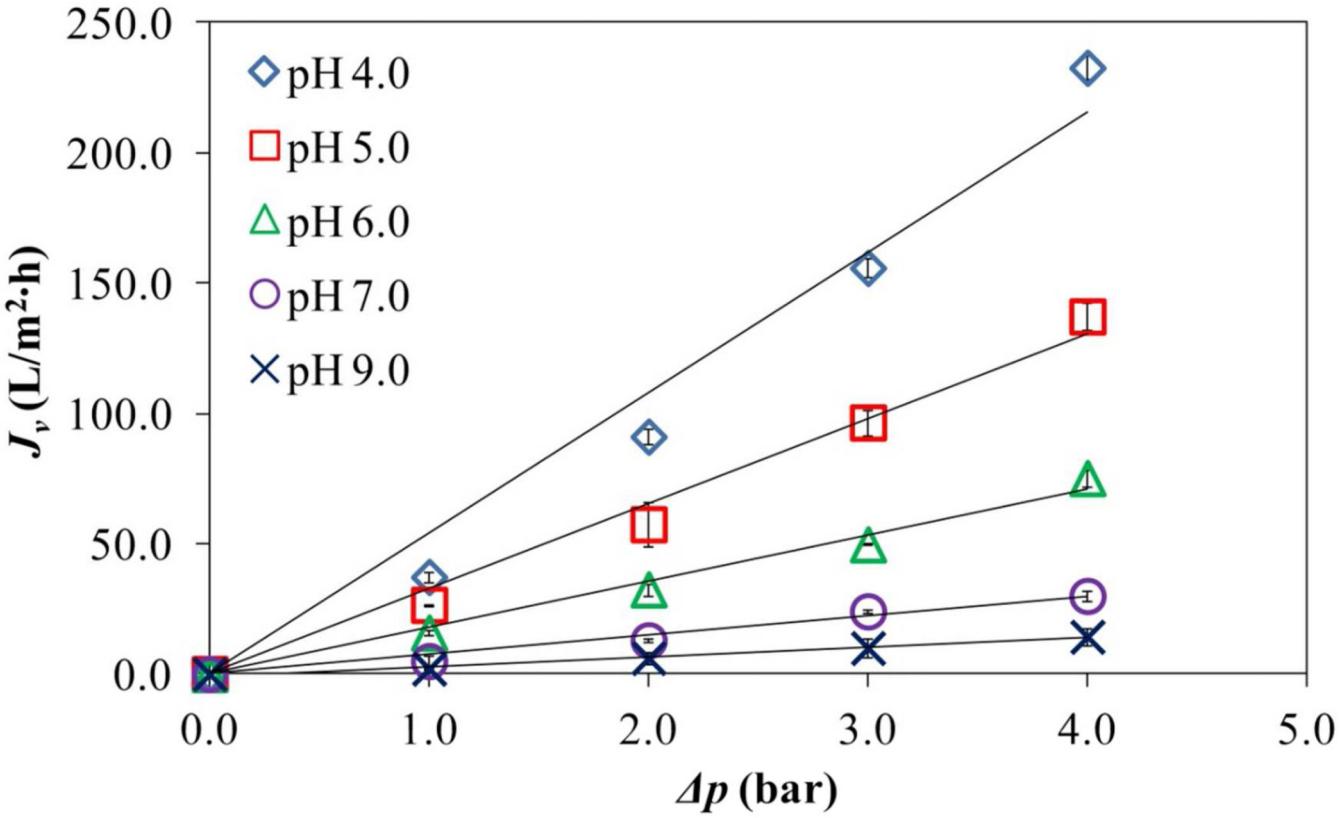


**Figure 14.**

pH responsive flux in PVDF-PAA membranes using convective cross-sectional flow. PAA content = 8.5% wt. Area PVDF-PAA membrane = 13.2 $cm^2$. Cross-linking, *X*= 1% NMBA. T = 22 °C

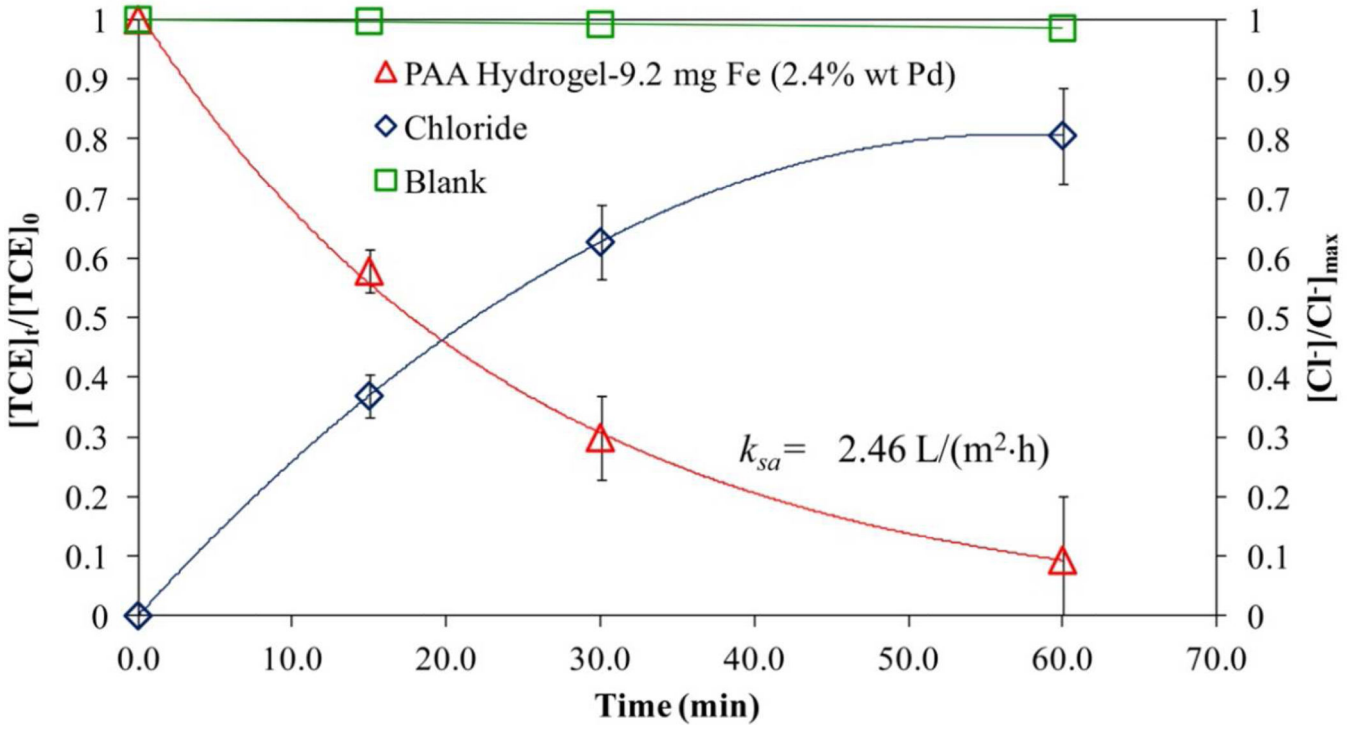


**Figure 15.**

TCE batch reduction by Fe/Pd nanoparticles supported in PAA hydrogel. TCE concentration = 0.21 mM. Volume = 0.12 L. pH ≈ 6.0. T = 22 °C.

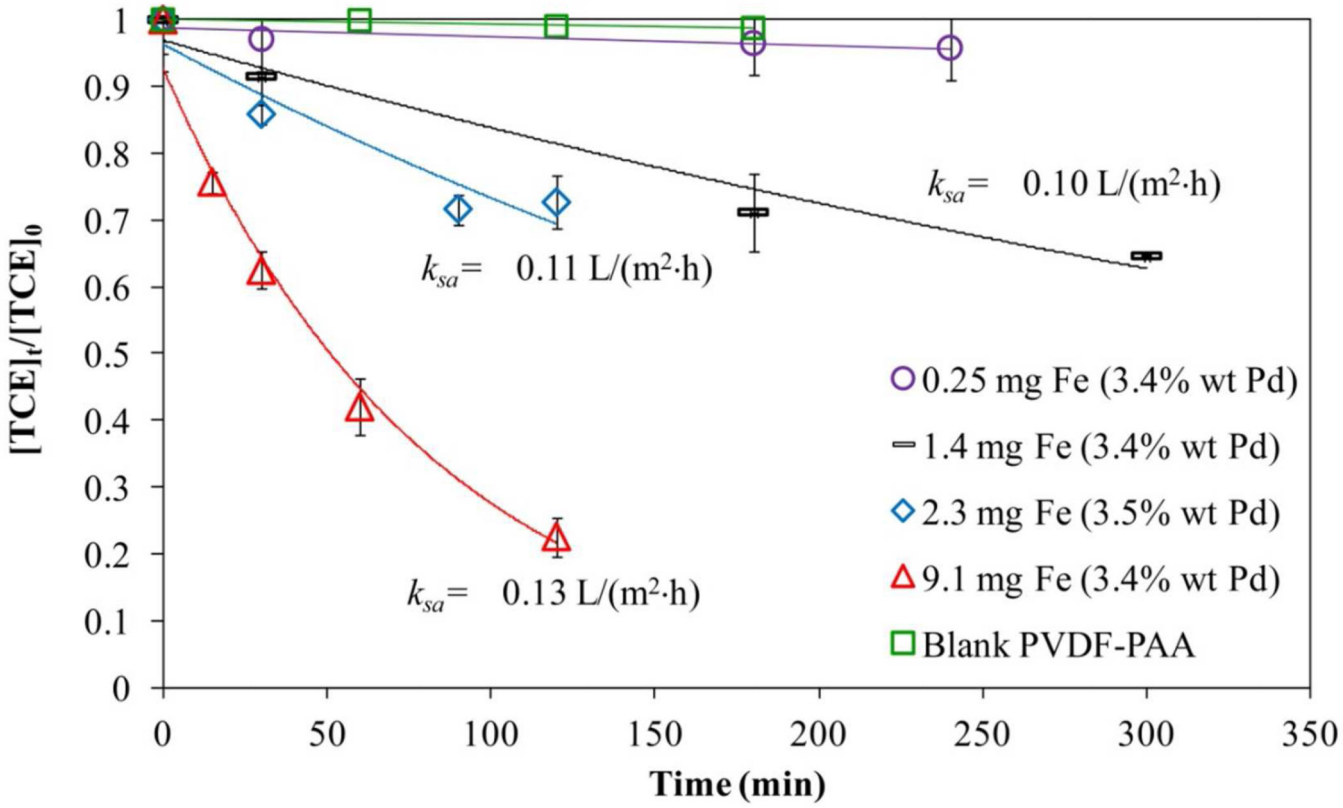


**Figure 16.**
TCE batch reduction by Fe/Pd nanoparticles supported in PVDF-PAA membranes. TCE concentration = 0.21 mM. Volume = 0.02L. pH ≈ 6.0. T = 22 °C.

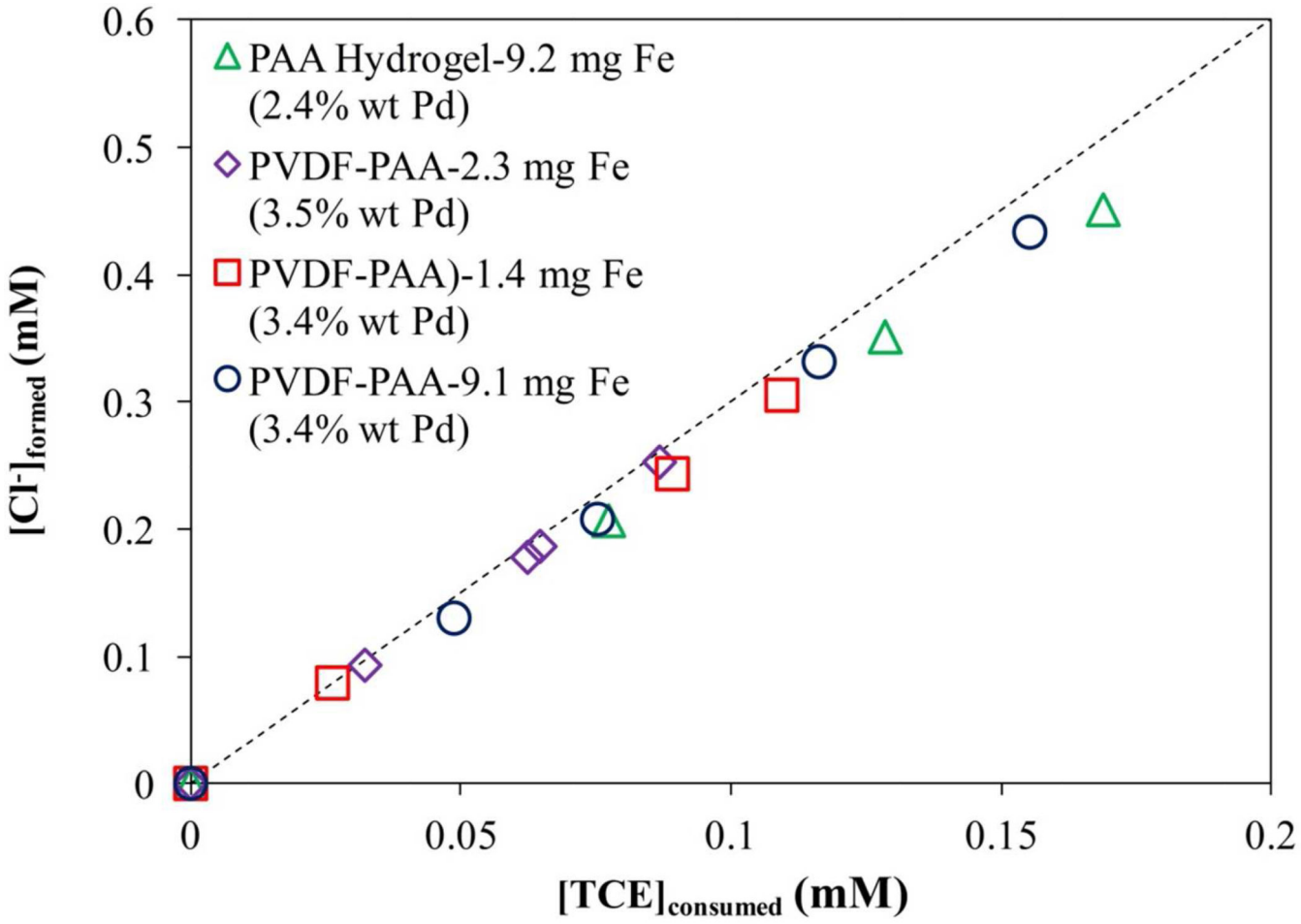


**Figure 17.**

TCE consumed in batch reduction by Fe/Pd nanoparticles and Chloride formation. TCE concentration = 0.21 mM. Volume = 0.02L. pH ≈ 6.0. T = 22 °C

## Table 1

Determination of iron species and total iron from polymerization in solution of AA (2.8 M at pH 3.0; $T_0$ = 22–25 °C) and Ion Exchange with $FeCl_2 \cdot 4H_2O$ (3.6 ± 0.04 mM; pH = 4.9); Area of membranes = 13.2 $cm^2$.

| Iron species | |
|---|---|
| Total Fe in hydrogel from polymerization | 9.2 ± 1.1 mg/g PAA |
| Total Fe in membrane from polymerization | 3.6 ± 0.3 mg/g PAA |
| $Fe^{3+}$ in membrane from polymerization | 91.7% |
| $Fe^{2+}$ in membrane from polymerization | 8.3% |
| Total Fe in hydrogel from ion exchange | 457.5 ± 8.1 mg/g PAA |
| Total Fe in membrane from ion exchange | 131.1 ± 3.1 to 428.3± 4.2 mg/g PAA |

**Table 2**

Determination of PVDF-PAA membrane equivalent pore diameters $d_p$ and permeability between high and low pressure conditions ($1.0 \leq \Delta p \leq 4.0$ bar; T = 22 °C) at different pH values. Area of membranes = 13.2 $cm^2$. Membrane thickness = 125 μm.

| pH | Dissociation degree of AA (%) | Permeability (L/($m^2$·h·bar)) | Pore diameter $d_p$ (nm) |
|---|---|---|---|
| 4.0 | 28.5 | 53.94 ± 7.59 | 222 ± 9 |
| 5.0 | 71.5 | 32.68 ± 3.39 | 198 ± 6 |
| 6.0 | 97.8 | 17.71 ± 1.28 | 171 ± 3 |
| 7. 0 | 99.6 | 7.44 ± 1.31 | 136 ± 7 |
| 9.0 | 99.9 | 3.39 ± 0.66 | 111 ± 7 |